OPTICAL MEMORY DEVELOPMENT

VOLUME II

Gain-Assisted Holographic Storage Media

BY

R. A. GANGE AND R. S. MEZRICH

INTERIM REPORT

NOVEMBER 1972

PREPARED UNDER CONTRACT NAS8-26806

RCA LABORATORIES
PRINCETON, NEW JERSEY 08540

GEORGE C. MARSHALL SPACE FLIGHT CENTER
NATIONAL AERONAUTICS AND SPACE ADMINISTRATION
HUNTSVILLE, ALABAMA 35812

1. Report No.	2. Government Accession No.	3. Recipient's Catalog No.
Interim Report		

4. Title and Subtitle	5. Report Date
OPTICAL MEMORY DEVELOPMENT Vol. II Gain-Assisted Holographic Storage Media	November 1972 6. Performing Organization Code
7. Author(s) R. A. Gange, and R. S. Mezrich	8. Performing Organization Report No. PRRL-72-CR-54
9. Performing Organization Name and Address RCA Laboratories Princeton, New Jersey 08540	10. Work Unit No. 11. Contract or Grant No. NAS8-26808
12. Sponsoring Agency Name and Address George C. Marshall Space Flight Center National Aeronautics and Space Administration Huntsville, Alabama 35812	13. Type of Report and Period Covered Interim Report 3/12/71 to 10/17/72 14. Sponsoring Agency Code

15. Supplementary Notes

16. Abstract

Thin deformable films were investigated for use as the storage medium in a holographic optical memory. The research was directed toward solving the problems of material fatigue, selective heat addressing, electrical charging of the film surface and charge patterning by light. A number of solutions to these problems were found but the main conclusion to be drawn from the work is that deformable media which employ heat in the recording process are not satisfactory for use in a high-speed random-access read/write holographic memory. They are, however, a viable approach in applications where either high speed or random access is not required.

17. Key Words (Selected by Author(s))	18. Distribution Statement
Holographic Storage Media Optical Storage Media Holographic Recording	

19. Security Classif. (of this report)	20. Security Classif. (of this page)	21. No. of Pages	22. Price*
Unclassified	Unclassified	84	

*For sale by National Technical Information Service, Springfield, Virginia 22151.

FOREWORD

This interim report was prepared by RCA Laboratories, Princeton, New Jersey for the George C. C. Marshall Space Flight Center of the National Aeronautics and Space Administration, Huntsville, Alabama. It describes work done under Contract NAS8-26808 during the period from March 12, 1971 to October 17, 1972 in the Information Sciences Research Laboratory, Dr. Jan A. Rajchman, Staff Vice President and Director. The Project Supervisor was Mr. R. D. Lohman. Members of the Technical Staff who participated in the research reported herein are Mr. R. A. Gange, Dr. R. S. Mezrich and Mr. G. W. Leck. Messrs. C. W. Robbins, C. C. Steinmetz, and G. E. Bodeep aided in in the fabrication of the devices. The NASA Project Monitor was Mr. E. J. Reinbolt.

It should be noted that about 50% of the effort described in this volume was supported by RCA Laboratories' funds under its parallel research program and the remaining 50% was supported by contract funds.

TABLE OF CONTENTS

TABLE OF CONTENTS (Continued)

TABLE OF CONTENTS (Continued)

LIST OF ILLUSTRATIONS

LIST OF ILLUSTRATIONS (Continued)

GAIN-ASSISTED HOLOGRAPHIC STORAGE MEDIA

by

Robert A. Gange and Reuben S. Mezrich
RCA Laboratories
Princeton, New Jersey 08540

SUMMARY

The objective of this research was to devise and investigate techniques for using deformable insulating films as the storage medium in a high-speed, random-access, read/write holographic memory. This included a search for solutions to the general problems associated with conventional thermoplastic-photoconductor systems, such as fatigue and uniform charging prior to exposure, as well as the specific problem of selective addressing, i.e., heating only one hologram area out of many thousands of such areas.

The fatigue mechanism was studied and a model was proposed that explained the failure of conventional thermoplastics. This model led to the discovery of a new material — microcrystalline wax — which was found to be free of fatigue up to at least 7000 cycles.

Improved corona-charging techniques were developed during the course of the work, and a method of charging with a space-charge-neutralized glow discharge was demonstrated.

The feasibility of selective heating by a light-addressed return electron beam was demonstrated, but problems with cesium contamination of the storage medium prevented the development of a practical operating device. Cesium induced conductivity of the insulating surface and also prevented photoemissive charge patterning.

A fundamental result of our research established the fact that no deformable film medium which uses heat to soften the material can be cycled at a frequency greater than the reciprocal of about 1000 times the heating time without excessive heat build-up at a location subjected to continuous erase-write operation.

A device consisting of a substrate, transparent conductor, photoconductor and a microcrystalline-wax insulating film was fabricated in which holograms were written over a 2 cm by 2 cm area by thermal biasing and direct laser-beam heating.

The main conclusion which we have drawn from this research program is that deformable media which employ heat in the recording process are not satisfactory for use in a high-speed random-access read/write holographic memory. They are, however, a viable approach in applications where either high speed or random access is not required.

I. INTRODUCTION

In recent years, substantial work has occurred in the field of holographic storage media. This work has been oriented toward the development of a material suitable for use in holographic data-storage systems. The requirements imposed on the storage medium by such a system have proven to be severe, as indicated by the fact that no material has been discovered to date which satisfies all of the requirements necessary for realistic system operation. By way of introduction to the progress achieved at the RCA Laboratories toward developing such a material, a brief outline is given below of the various requirements imposed by the system on the storage medium.

A. Write Sensitivity

In a practical system laser power is at a premium; present laser technology provides for power of the order of 1 to 10 W in a useful line (single frequency) of reasonable coherence. If σ denotes the system loss in laser light through the deflector, hololens, optical components and page composer, and h denotes the diameter of the hologram at the storage medium, then the sensitivity S required of the storage medium (J/m^2) is

$$S < \frac{4e\sigma}{\pi h^2} \tag{1}$$

where e is the available laser energy. The hologram dimension at the storage medium equals the diameter of the Airy disk $\sim 2\lambda L/b$ (rectangular aperture), with λ the wavelength of the laser light, L the focal length of the lens, and b the width of the page composer and photodetector elements. Since the area of the page composer $\pi\beta^2/4$ (β = page composer diameter) equals $(bN/\eta_{PC})^2$, where N^2 is the number of bits per page and η_{PC} is the spatial duty factor of the page composer elements, it follows that $\pi h^2 = (8\lambda LN/\beta\eta_{PC})^2$. Noting that L/β is the F-number (#) of the lens, the system requirement on storage material sensitivity is

$$S < e\sigma \left(\frac{\eta_{PC}}{2\lambda \# N}\right)^2 \tag{2}$$

B. Read Efficiency

In addition to adequate write sensitivity, the storage material must be capable of diffracting the light sufficiently for adequate signal to noise at the detector. If g is the minimum energy per bit necessary at the detector, τ_p the reading time and P the average available read power, then the readout efficiency (f) of the storage material must be such that

$$f > \frac{gN^2}{P\tau_p\sigma} \tag{3}$$

C. Material Fatigue

A material suitable for holographic read/write storage must be able to have information written and erased without any appreciable change in the material's properties. The inability of traditional thermoplastic type materials to maintain molecular integrity during repetitive electrical alteration of their information content has proven to be a formidable problem area. In typical read/write memory operation, such fatigue raises the temperature required to write information into the storage material. In traditional materials, a thermoset temperature is reached beyond which the medium ceases to operate as a holographic storage material. The onset of this fatigue is irreversible and may typically occur anywhere between ten and several hundred read/write cycles. Clearly, the absence of such fatigue is a major requirement on any storage material for use in an electrically alterable holographic-memory system.

D. Spatial Resolution

Information is written into the storage medium by spatially modulating one of two coherent laser beams, and superimposing these beams at the desired storage location. The beams interfere and produce an intensity (I) with a spatial variation of the form

$$I = I_o \left[1 + \cos kx \left(\sin \theta_1 + \sin \theta_2\right)\right] \tag{4}$$

where I_o is some constant, $(\theta_1 + \theta_2)$ the angle between the two beams, k the wave number of the laser light, and x the distance along the surface of the storage material. Equation (4) shows that the storage material must be able to respond to spatial variations whose period D is of the order of

$$D \sim \lambda/(\sin \theta_1 + \sin \theta_2) \tag{5}$$

where $\lambda = 2\pi/k$ is the wavelength of the laser light. Analysis of the resolution one obtains upon reconstruction of the stored image shows that for typical object and system dimensions, $(\theta_1 + \theta_2)$ is of the order of $\pi/6$ to $\pi/4$ radians so that the storage material must be capable of retaining spatial variations of the order of the wavelength (λ) of the laser light. This material bandwidth requirement also restricts the thickness of thermoplastic materials (ref. 1) to a maximum value of about D/2.

E. Temporal Response

Another requirement which the system places on the storage bandwidth is that of temporal bandwidth. The cycle time of the memory includes both the erase time and the write time as well as the read time. In storage media using heat, the heating and cooling times must also be considered.

F. System Compatibility

A requirement often overlooked in the choice of a material for holographic memory applications is the compatibility of the material with the system in which it is going to be used. For example, a storage material may have adequate write sensitivity in terms of energy, but require the application of this energy in time intervals not realizable with existing or forseeable laser technology. Another example is materials which may satisfy all of the storage requirements, but which have a spectral response either in the infrared or ultraviolet part of the spectrum where deflector or detector incompatibility may exist. Perhaps the most often encountered example of system incompatibility is where the material satisfies all of the definable criteria, but does so only over areas of the order of square millimeters. In such an instance, the requirement for areas of many square centimeters proves to be a formidible, if not impossible task.

G. Summary

The requirements imposed by the system on a holographic-storage material as discussed above have proven to be formidable. Of the various kinds of materials considered for use in situ in a read/write holographic optical memory, thermoplastics have emerged as a possible candidate. Such materials have been extensively investigated at RCA Laboratories, and have been found to satisfy some of these requirements. Therefore, a brief description of the use of thermoplastic materials for recording holograms is given in the following section.

II. THERMOPLASTICS

A. Introduction

The deformation of thermoplastic materials in response to patterns of electrical charge on their surface dates back to 1897 (ref. 2). During the past twenty years these deformations have been investigated by many workers (refs. 3-18). The use of thermoplastic materials for holographic storage was first demonstrated by Urbach and Meier in 1966 (ref. 13).

The recording of a hologram in a thermoplastic material is done by introducing spatial variations in the thickness of the thermoplastic film. The thickness variations correspond to differences in the laser-light intensity of a holographic fringe pattern. The thermoplastic is usually a resin type material which is insensitive to light. Therefore, it is normally used in combination with a sensitive photoconductor such as poly-N-vinylcarbazole (ref. 19).

B. Device Configuration

A typical thermoplastic-photoconductor film storage device is shown in Fig. 1. The thermoplastic-photoconductor combination is placed over a transparent electrode such as tin oxide (TIC) or indium oxide (InO). This transparent electrode acts as a ground plane to image charge of polarity opposite to that placed on the surface of the thermoplastic material. It is the electrostatic force between the charge on the thermoplastic surface and the corresponding charge imaged in the ground plane which causes the thermoplastic material to deform.

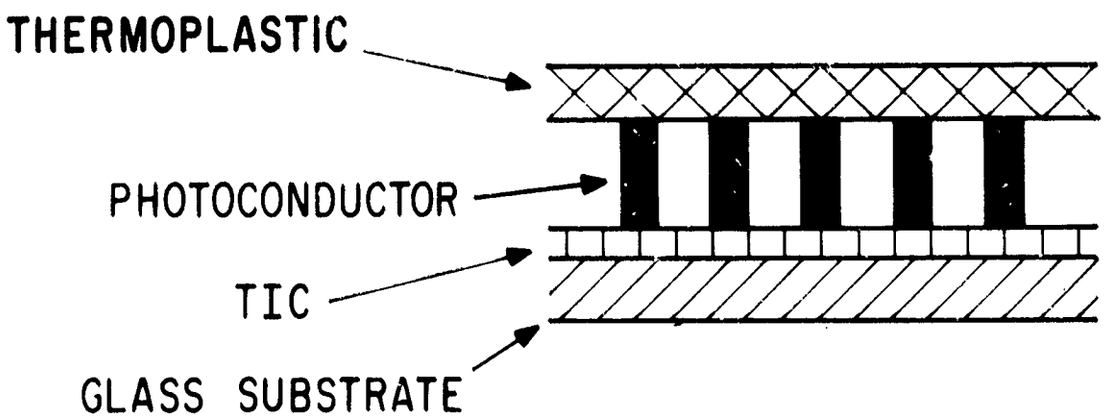

Figure 1. Thermoplastic-photoconductor film storage device.

C. Corona Discharge

A corona device consisting of a thin wire or wires at high voltage (~10 kV), and an electrically grounded shield is usually employed to charge the thermoplastic surface. The fine wire ionizes the air because of the high electric field strength in its proximity. The ions are attracted to the thermoplastic surface because of the electrically grounded transparent conductor. The ions are deposited onto the thermoplastic surface and held by the charges induced in the transparent electrode. Thus, the surface of the thermoplastic material is charged to a uniform potential which typically is several hundred volts.

D. Hologram Write Procedure

For ease of visualizing the storage of a hologram in a thermoplastic material a recording sequence is described below and illustrated in Figs. 2A-E.

In Fig. 2A, the thermoplastic surface has been charged positive by a corona-type device, and is at a uniform potential. The corona is then turned off.

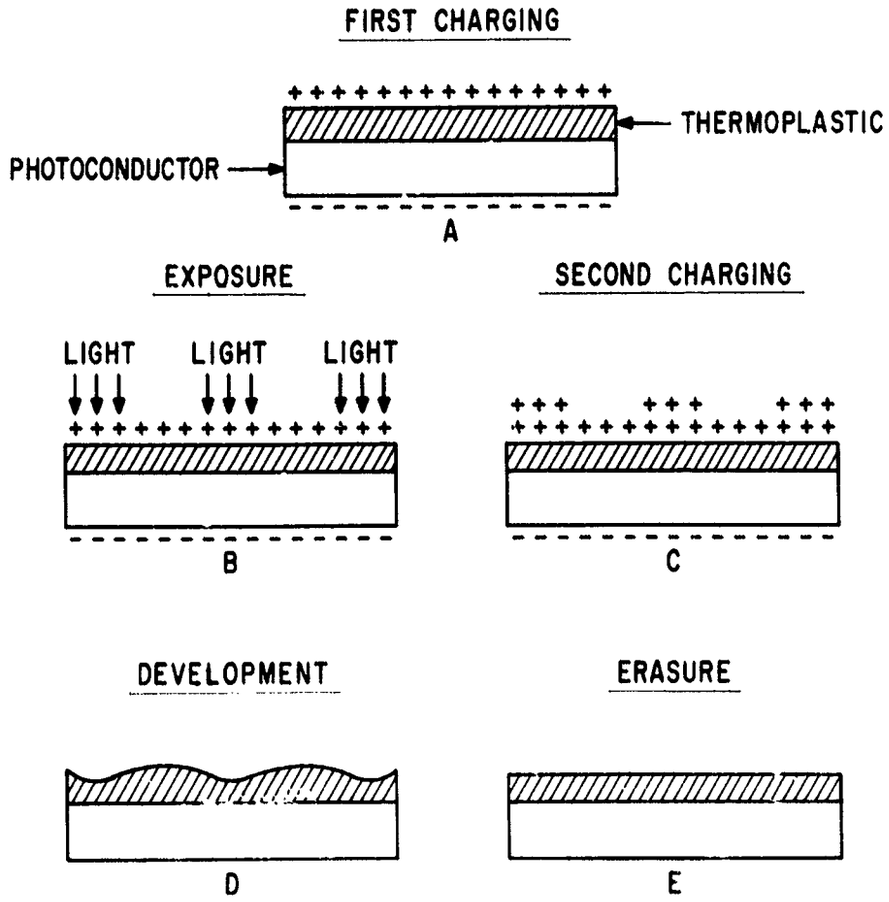

Figure 2. Thermoplastic hologram recording sequence.

Figure 2B shows the distribution of charge within the photoconductor layer subsequent to exposure by two laser beams, which have been made to interfere with one another. The effect of the light is to excite charge carriers within the photoconductor, where they are then free to move toward the thermoplastic-photoconductor interface under the force of the charged thermoplastic surface.

In Fig. 2C, the corona-charging device has again been turned on, and a new layer of charge deposited on the thermoplastic surface. The newly deposited charge distributes itself along the surface in a manner which allows the total electrostatic energy to assume a minimum value. Figure 2C shows the distribution of charge which corresponds to this minimum energy configuration, and although a greater amount of charge is seen to accumulate in regions of high light exposure, the surface is at a uniform potential. The corona discharge is removed subsequent to application of this second layer of charge.

Figure 2D shows the configuration of the thermoplastic surface after momentarily applying heat to the thermoplastic material. The heat raises the temperature near the softening or melting point and the regions of higher charge accumulation and therefore higher electric field strength deform under the action of the greater attractive force which exists between the negative-imaged electrode charge and the positive thermoplastic surface charge. The thermoplastic material thus deforms in accord with local electric field strengths, and becomes thinner at the high field (illuminated) areas, but thicker elsewhere. As the heat leaves the composite structure, the thermoplastic cools to room temperature where the thickness variation remains as a permanent deformation. The hologram is thus recorded.

E. Hologram Erase Procedure

Figure 2E shows the storage structure subsequent to the reapplication of heat in the absence of corona discharge and light exposure. The reapplication of heat raises the temperature of the thermoplastic material to a value higher than that used to record the hologram. At this higher temperature, the thermoplastic material is restored to its initial smooth configuration under the action of surface tension forces. The reapplication of heat in the absence of corona discharge and light exposure thus corresponds to erasure of the previously recorded hologram. In addition, any remanent charge which may exist on the thermoplastic surface is removed during erasure because of the increased electrical conductivity of the thermoplastic and photoconductor at the elevated erase temperature.

III. FATIGUE

A. Introduction

The recording and erasure of a hologram in thermoplastic materials as outlined in Figs. 2A-E is seen to occur at specified softening or melting temperatures achieved by the transfer of heat to the storage material. Since many holograms exist in an optical memory system side by side on a common film, a change in the softening or melting temperature at any one hologram location makes it essentially impossible to write holograms over the entire storage medium with a constant heat energy. In the extreme, the melting temperature is higher than the temperature at which the material is destroyed. At intermediate temperatures, loss in the plasticity necessitates progressively greater values of electrostatic force to deform the material. This change in the softening or melting temperature is called fatigue. It usually occurs as a result of polymerization and crosslinking at the molecular level.

Other mechanisms can also produce material fatigue. For example, tree resins such as staybelite are believed to fatigue due to oxidation at the surface of the film. This oxidation ostensibly occurs prior to the onset of any appreciable polymerization and crosslinking, and therefore is believed to be the dominant fatigue mechanism in tree resins such as staybelite.

B. Frost Temperature

In order to investigate the fatigue mechanisms in polymer type materials, and to identify those factors which contribute to material degradation during the repetitive writing and erasure of holograms, work was initiated on the study of frost temperatures of styrene fabricated in varying stages of virgin polymerization. The frost temperature of a material is the temperature at which one observes the onset of scattering from a single beam of laser light made to fall uniformly over some region of the sample in the presence of a uniform corona discharge. Such scattering, or "frost" as it is commonly called, is observed to occur with substantially all thermoplastic materials.

C. Frost Mechanism

A mechanism believed to be responsible in part for the phenomenon is the inverse dependence of surface tension on the electrostatic potential at the thermoplastic surface due to lateral repulsion of like charges. In an analogy to the electrocapillary effect (ref. 20), the change in surface tension δS may be expressed to a first-order approximation as the product of the surface charge density (σ) times the mean-surface potential (ϕ) measured from the transparent electrode.

D. Mechanical Versus Electrostatic Stress

If the change in electrostatic energy corresponding to the thickness variations in the thermoplastic is calculated under the assumption of a single harmonic mechanical contour, then it can be shown that the change in surface energy δS is more accurately given as

$$\delta S = \frac{\sigma^2/kK}{K + \tanh kh} \tag{6}$$

where k, K, and h are the mechanical wave number, dielectric constant, and separation from the transparent electrode of the thermoplastic material. Since the total energy is a minimum value, δS is a measure of the negative of the change in mechanical energy by which the thermoplastic is mechanically stressed. Thus, the thermoplastic is seen to mechanically deform in the presence of both heat and electric field intensity with maximum stress occurring at maximum field strengths.

E. Polymerization and Crosslinking Versus Frost Temperature

1. Deposition procedure. — In order to evaluate the effect of heat and electric field intensity on the elastic properties of polymers, styrene films were fabricated with structures containing different degrees of polymerization and crosslinking. The polystyrene films were fabricated by polymerizing styrene molecules in a vacuum system. The initial rough-down prior to introducing styrene into the system was done at a pressure of about 1 μm. The styrene monomer [maximum vapor pressure = 3000 μm (3 torr)] with an additive (tert. - Butylpyrocatechol) for stability was bled into the vacuum system such that 100% evaporation yielded a pressure within the bell jar of about 150 μm (.15 torr). The pressure was then increased to 500 μm (.5 torr) by bleeding air into the system. The styrene films were deposited on transparent TIC electrodes placed between two parallel, circular, stainless-steel plates each 750-μm thick, and separated from one another by about 2.5 cm. The energy necessary to polymerize (and crosslink) the styrene monomer was supplied by an alternating electric field generated by placing a 60 Hz — 480 VRMS voltage across the parallel circular plates through a 4000-ohm resistor. During the polymerization process, a blue-glow discharge (not an arc) is observed, and the activation (0.3 eV) to ionization (3.0 eV) energy ratio of 1:10 is believed to produce a ratio of styrene activated to ionized monomer molecules of 10^6:1; random collisions between the plates are rare, and the styrene polymerization is felt to occur because of the increased collision probability associated with higher retention times at the surface of the conductive films. Electrical contact was made to the transparent electrodes as shown in Fig. 3. The glass substrate was placed on a gold-plated 5-cm by 5-cm copper block, and a wire from a clip lead placed on the transparent electrode was soldered to a copper block which rests upon the lower plate. Styrene was simultaneously deposited upon as many as eight 5-cm by 5-cm samples; however, since the electric field exists between the upper and lower circular plates, as well as between the upper plate and metallic film, the styrene is deposited on the lower plate as well as the sample. Thus, regardless of the particular number of samples employed during a given styrene

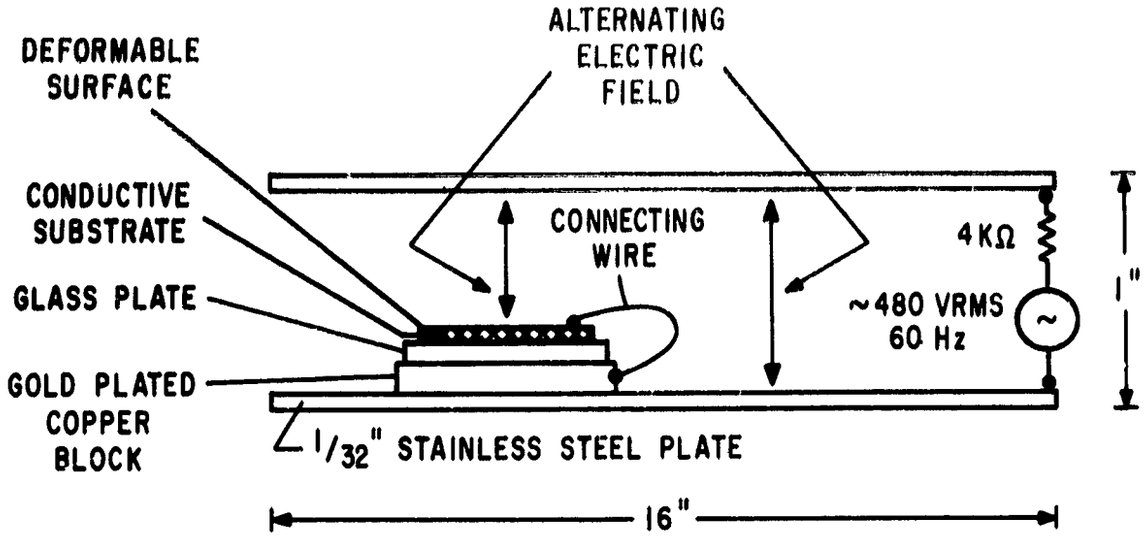

Figure 3. Sample connections during styrene deposition.

deposition, eight copper plates must be positioned in the eight locations initially established on the lower circular plate; otherwise, these regions will be coated with styrene and electrical contact between the copper blocks and the lower circular plate upon which the blocks rest will be lost.

2. Molecular saturation control. — The high energy of molecular formation produces multiple crosslinking as well as polymerization of the styrene monymer molecules. The increase in pressure to 500 μm (0.5 torr) by the addition of air was used to control the extent of the crosslinking. Although most of the samples fabricated contained 240-nm-thick polystyrene films, devices with styrene thicknesses between 160 nm and 320 nm were also evaluated. A 10-microliter volume of styrene monomer typically produces an 80-nm film over a 2581-cm^2 area (upper and lower plates). Typical power consumption during the polymerization process decreases from an initial high of 5 mW/cm^2 to 0.5 mW/cm^2, with the initial 480 VRMS decreasing to about 300 VRMS, and the initial 55 mA current increasing to 70 mA. The decrease in power results from the growth of the styrene film over the sample and plate areas. In high electric-field regions, the film is believed to grow in a macromolecular fashion with an entire coating along one strip possibly being one large molecule. It is noteworthy that the solubility of such compounds is inversely proportional to the molecular weight, and that these coatings remain substantially unaffected when exposed to conventional styrene or polystyrene solvents; this suggests molecular weights appreciably in excess of that normally associated with conventional polystyrene.

3. Complex styrene analysis. — Mass spectrometer measurements were taken of vapor pressure in which the complex styrene coatings were placed in a chamber, evacuated, the pumping stopped, and the evolved species collected over a 15-minute period. Spectra were obtained from this sampling

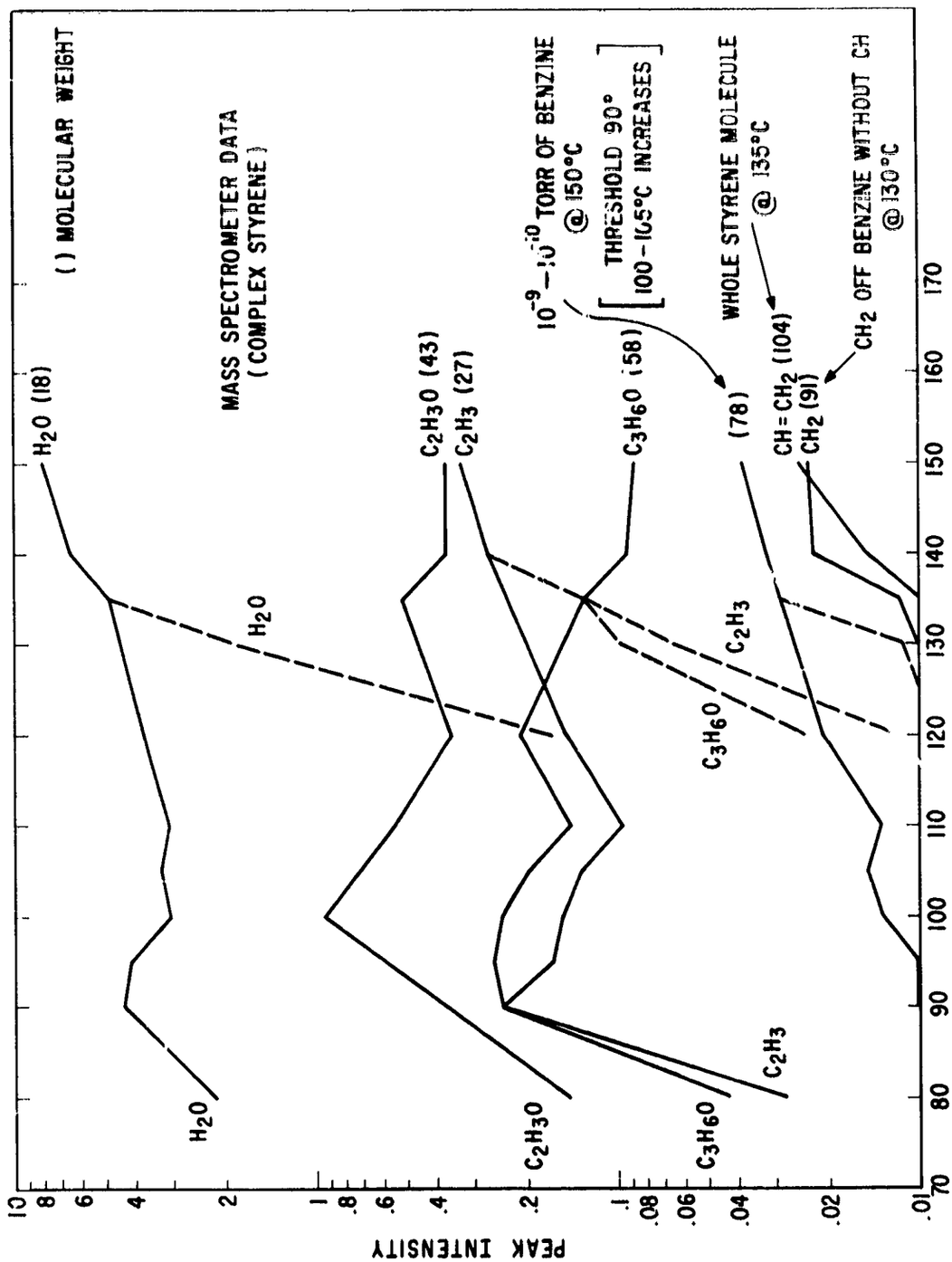

Figure 4. Complex styrene mass spectrometer data.

procedure at 27°C, 54°C, 85°C, 110°C, 125°C, 148°C, 156°C, 179°C, and 210°C. Figure 4 shows data taken from mass spectrometer measurements illustrating the evolved species, and showing that styrene coatings deposited in maximum field strength regions are quite stable up to temperatures of 90°C. Whereas an enticipated spectra was observed under a similar measurement with ordinary polystyrene at about 100°C, quantitatively small species were evolved from the styrene coatings deposited in high-field regions, even at 210°C. The species detected were only slightly above the detection limit which is on the order of 10^{-7} to 10^{-8} μm (10^{-10} to 10^{-11} torr). At room temperature there was evidence of a C_4H_8 species with a terminal CH_3 group. Another species detected was a C_3H_5 group. Figure 5 illustrates a structural configuration of the polymerized and crosslinked styrene coatings which is reasonably in accord with the evolved detected species, although other equally viable structures can be hypothesized.

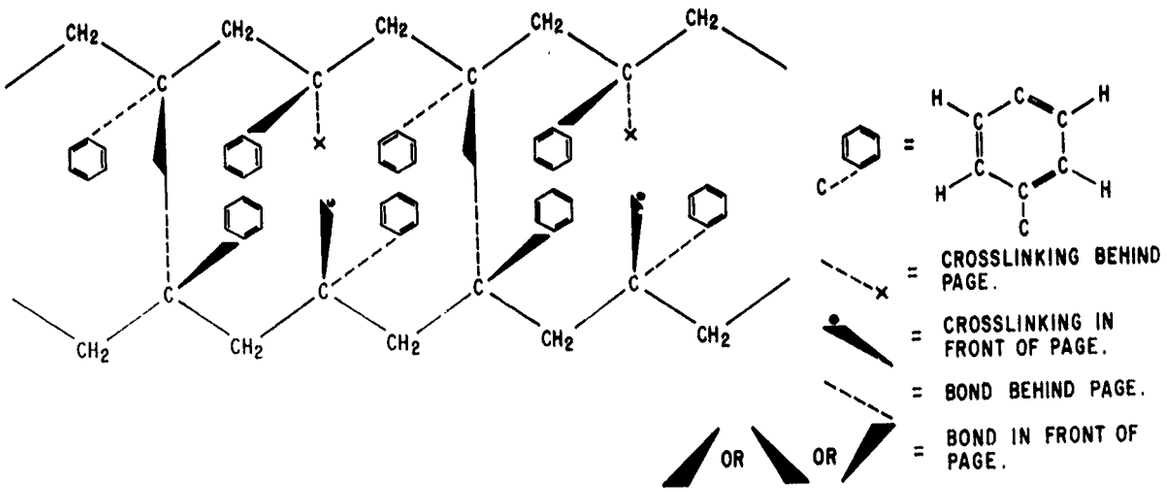

Figure 5. Complex styrene structural configuration.

4. Molecular saturation versus electric field. — The variation in the polymerization and crosslinking present within the styrene films was achieved by means of glass substrates on which were etched seven strips of TIC (transparent electrodes). The glass samples were placed on top of the gold-plated copper blocks as shown in Fig. 3, but electrical connection was made to only the center strip. In this way, the electric field intensity between the upper plate and the strips was a maximum over the center strip and a minimum in the region of the TIC strips furthest removed from the center of the sample. The technique for interconnection along with an illustration of the relative field strengths is depicted in Fig. 6. The decrease in electric field intensity from the center strip and along the three unconnected strips on either side serves to produce a gradient of molecular saturation with a substantially higher degree of polymerization and crosslinking in the styrene deposited along the strip at the center of the glass substrate, and lesser degrees of polymerization and crosslinking occurring in rough proportion to the separation of the strips away from the center strip, i.e., the point of electrical connection.

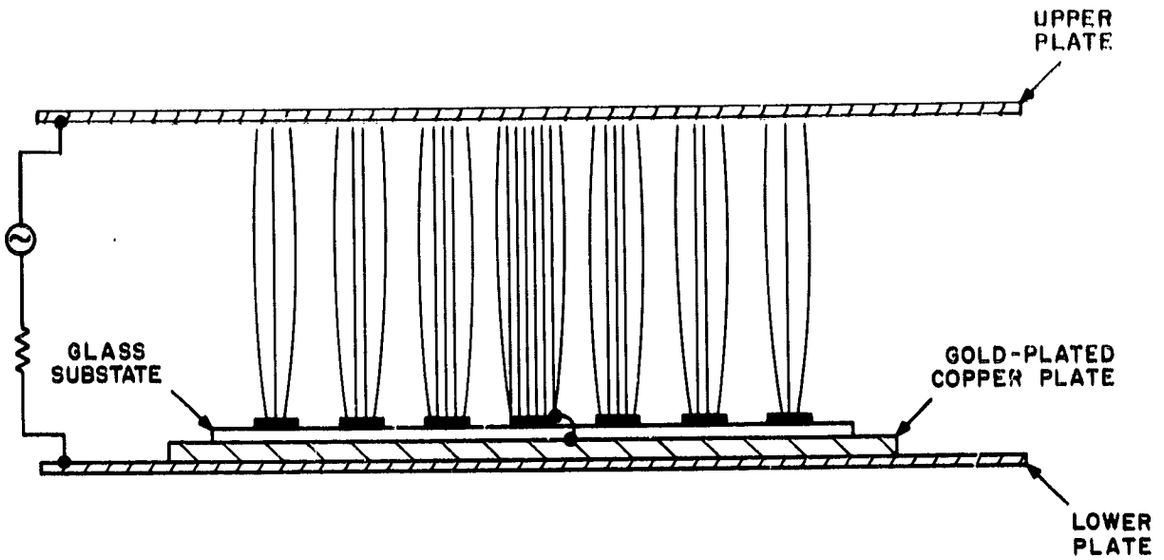

Figure 6. Electric field strength vs. electrode strip position.

5. Test Data. — Tests were later conducted to investigate the effect of ohmic-heat and corona-discharge-induced electric fields on the frost temperatures of the different strips. Figure 7 typifies the distribution in frost temperature versus strip position which was observed. Styrene deposited on strips furthest removed from the region of maximum electric field strength exhibited frost at lower temperatures ~35°C, while styrene on strips in close proximity to the maximum field region frosted at higher temperatures ~50°C. No frost was observed at any time on styrene coatings deposited on the center strip, the region of maximum field intensity at temperatures up to ~100°C.

6. Electric field induced fatigue. — A significant discovery was that whereas the strips could be heat-cycled between room temperature and ~50° with no significant change in the temperature at which frost occurred, subjecting the strips to about five cycles of corona discharge (depending upon corona intensity) in each instance raised the frost temperature until, at a temperature of ~70°C the frost was permanently frozen in. Thus, regardless of the initial state of polymerization and crosslinking and the initial frost temperature, except for the center strip at which electrical connection was made, each strip suffered an increase in the temperature at which frost occurred, with the styrene exhibiting permanent frost at ~70°C.

The increase in the frost temperature of the incompletely saturated coatings is attributable to increased polymerization and crosslinking due to the corona discharge. The permanent frost condition derives from a thermoset condition of the styrene resulting from a saturation of the polymerization and crosslinking due to depletion of available covalent bonds. These results appear to be of general character, applicable to most crosslinked polymers. Additional work with resins and rubbers at RCA Laboratories and reported in later paragraphs support this conclusion.

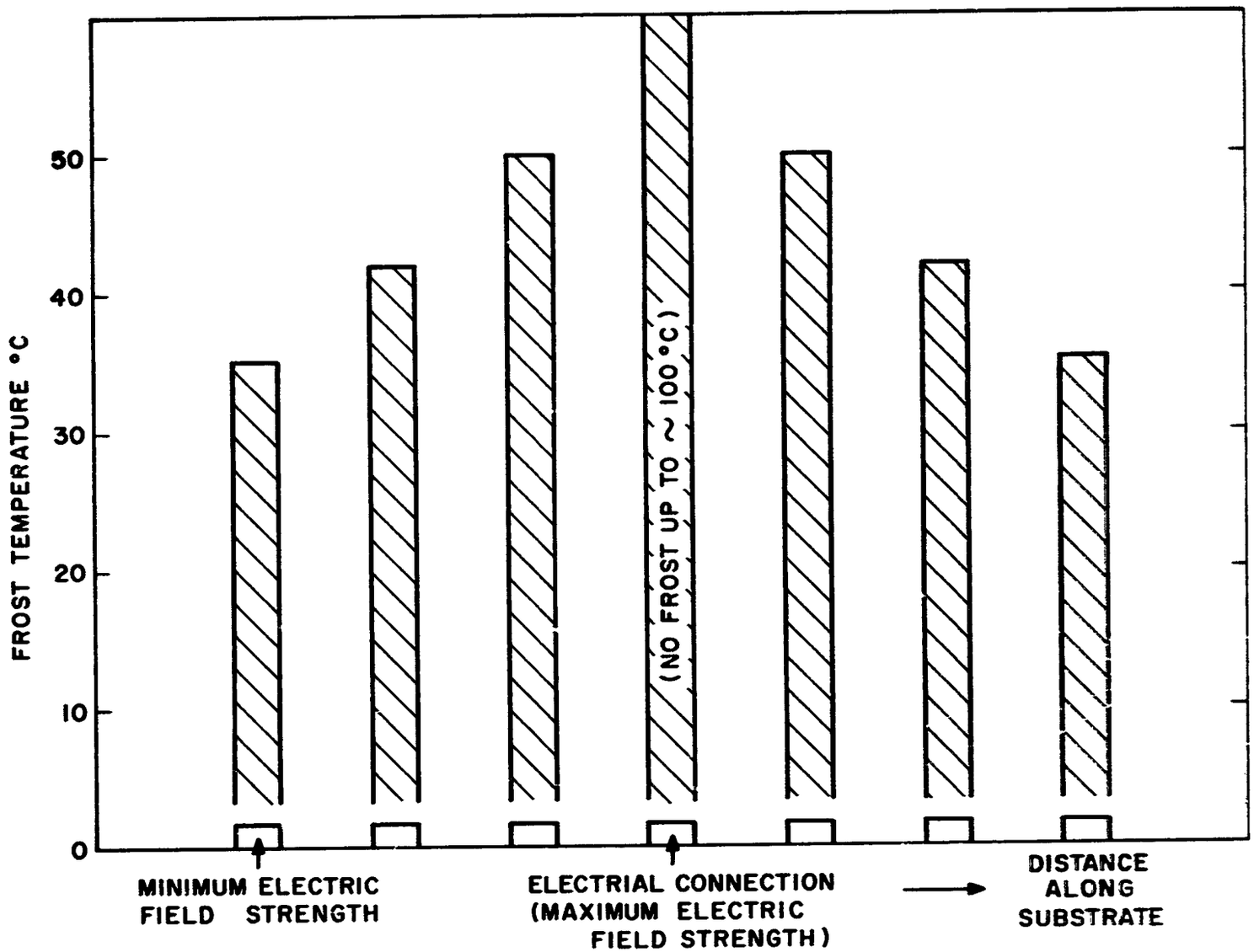

Figure 7. Frost temperature versus strip position.

F. Complex Styrene Structure

Work was also done to evaluate the electric-field-induced structure of the highly crosslinked complex styrene films. The styrene coatings were investigated using x-ray diffractometery, electron diffraction, differential thermal analysis, and mass spectrometry. The results from these tests were consonant with one another, and showed the "complex" styrene films to contain an amorphous structure of approximately 5-nm polycrystallite (see Fig. 8), a glass transition and melting temperature respectively, of 146°C and 205°C, and a vapor pressure at 90°C of 10^{-8} μm (10^{-11} torr), and at 150°C of ~5×10^{-7} μm (~5×10^{-10} torr). The high transition and melting temperatures explain why frost was not observed in the center strip, and why it appeared to be frozen in at ~70°C. The data also shows that the complex styrene coatings are quite amenable to high vacuum use, an application of which more will be said with regard to work on photoemission.

G. Inhibition of Polymerization and Crosslinking

In an attempt to prevent covalent band saturation via polymerization and crosslinking, styrene films were deposited using the vacuum system of Fig. 3 in which an additive was introduced during styrene deposition. A 0.85 styrene -0.15 octyl-decyl metacrylate composition monomer admixture was introduced in an attempt to plasticize the film in the absence of solvents. The use of solvents to plasticize styrene films has been shown to be detrimental to organic photoconductors of the kind employed in holographic-storage devices. For this reason, a glow-discharge technique was selected for the monomer admixture. However, in spite of every precaution, and using several fabrication procedures, sufficient polymerization and crosslinking occurred during deposition to render the styrene coatings non-deformable at practical temperatures $\lesssim$ 120°C.

H. Fatigue in the Absence of Heat

1. Materials selection. — Conclusions regarding the fundamental mechanisms by which fatigue occurs in polymer materials indicated that these mechanisms should be present in polymers deformable at room temperature. Although fatigue studies embraced a wide spectrum of materials including monomeric amides, lacquers and resins, an investigation was initiated to study the effect of electric fields from a corona discharge on elastomers.

Dow Corning silicon elastomer #236 (dispersion) was selected because of the ease with which it deformed at room temperature. At no time was it necessary to apply heat to the material, and the corona discharge was the only external energy source to which the material was exposed. The silicone elastomer was applied to TIC coated glass substrates using both dip and spin type coating techniques. The range in film thickness was varied from 1 to 15 μm, with most tests conducted on coatings between 1 and 3 μm. Figure 9 shows the device structure.

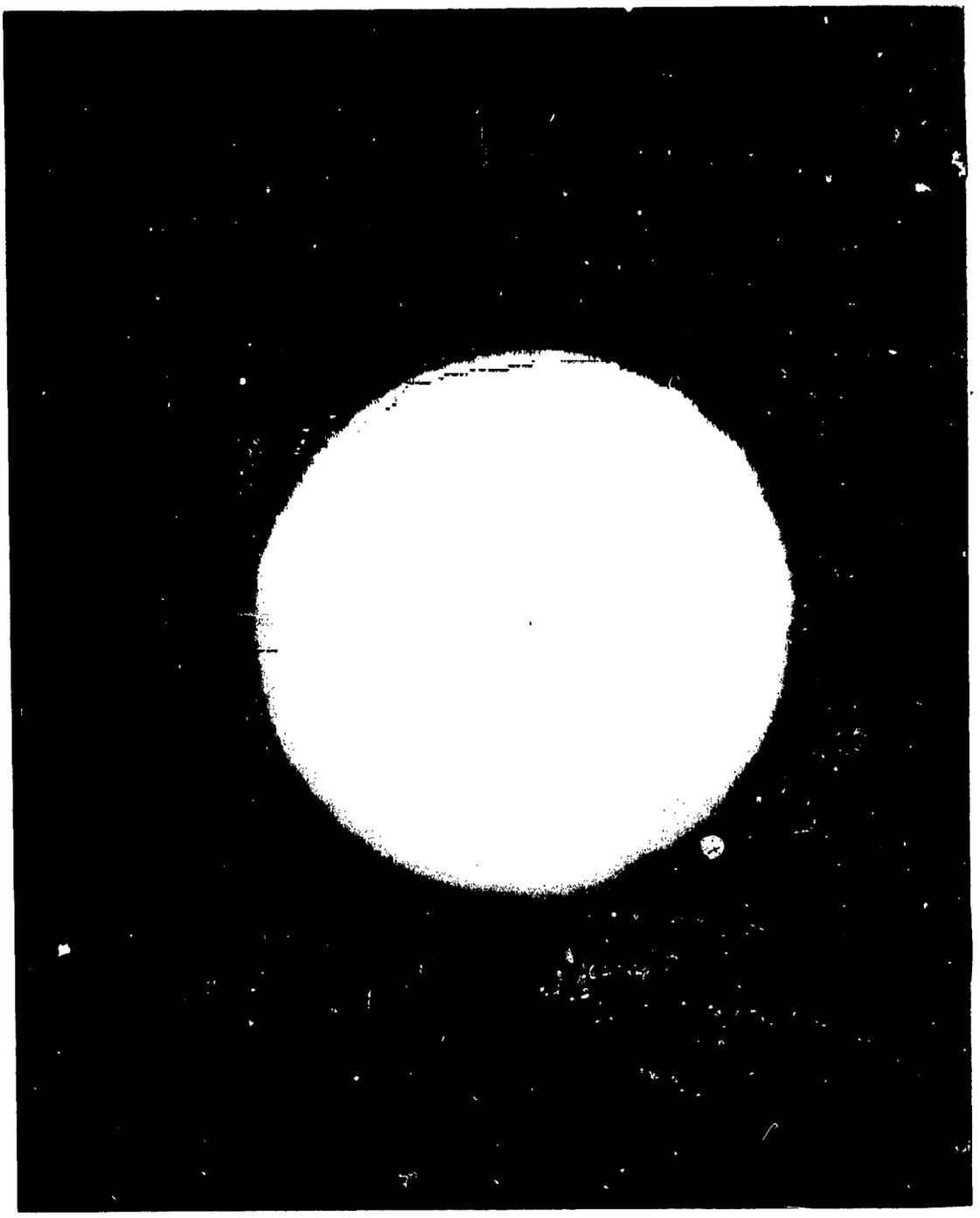

Figure 8. Complex styrene electron diffraction pattern.

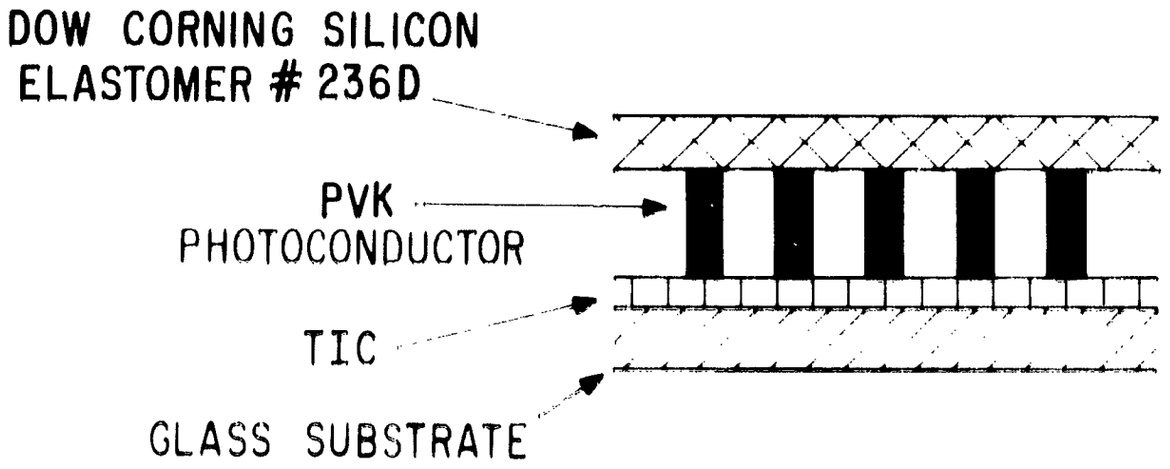

Figure 9. Silicone #236 dispersion device structure.

2. Experimental arrangement. The experimental arrangement used during the course of the investigation is shown in Fig. 10. He-Ne (6328Å) laser light of about 1 mW power was made to fall on a beam splitter, and part of the beam (Beam B) to be deflected onto a mirror. Beams A and B were then made to superimpose on the sample at an angle of about 5 °, with Beam A orthogonal to the

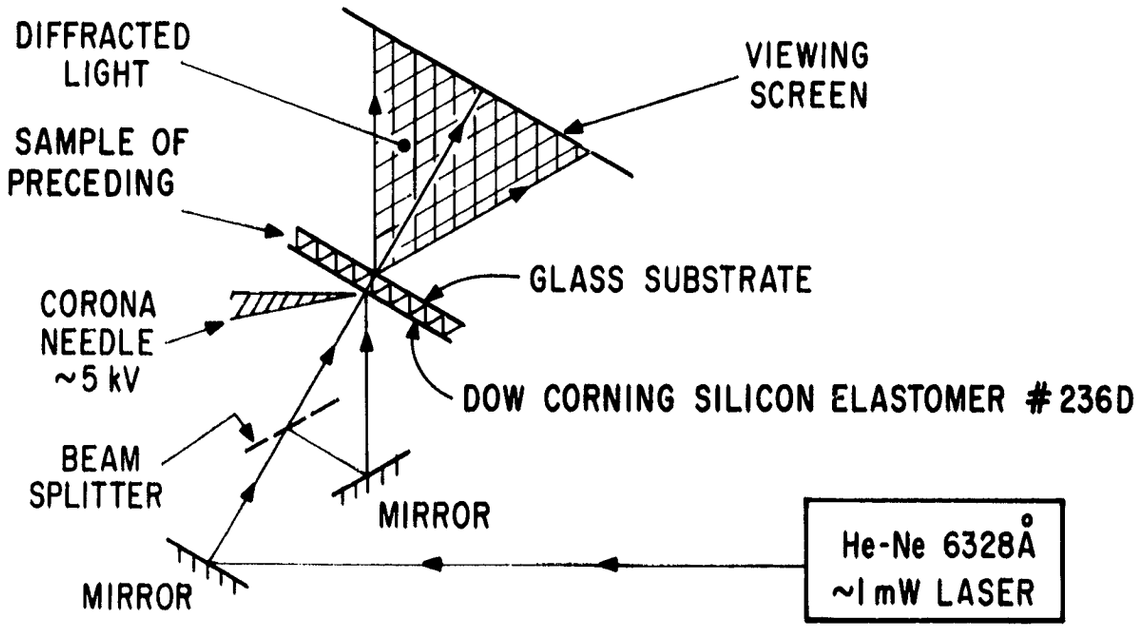

Figure 10. Experimental arrangement for silicone hologram recording.

surface. The higher order readout beams were viewed at a later time on a white screen placed at a distance of about 15 cm behind the sample using only Beam A. During exposure to the corona discharge, the charge distributed along the interface between the PVK and the elastomer in a one-to-one relationship to the interference pattern made by overlapping two laser beams on the PVK-deformable coating sandwich. The differential forces produced by the unequal charges produced holographic surface deformations which diffracted the laser light.

3. Experimental data. Figure 11 is a 130X photograph (using oblique lighting) of the surface of Dow Corning #236 dispersion silicone elastomer subsequent to exposure by the corona discharge. The figure shows that the surface deformations have been permanently stored in the silicon elastomer. The experiment thus conclusively demonstrated that in the absence of heat, application of the corona discharge caused permanent fatigue to the partially polymerized and crosslinked silicon elastomer, in accord with the conclusions drawn earlier from work employing styrene as the deformable material.

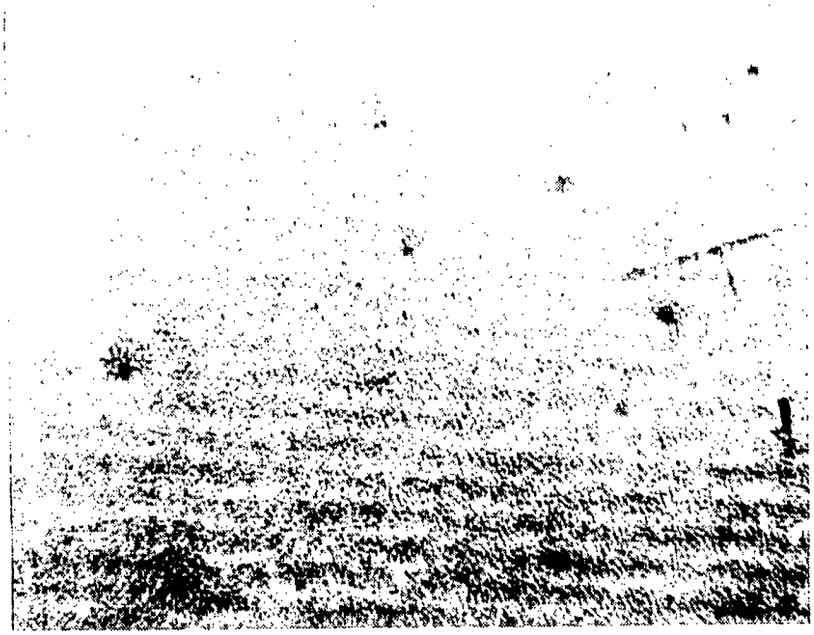

Figure 11. Grating permanently stored in Dow Corning #236 dispersion.

4. RTV 619. — In order to evaluate the role played by the electric fields in the fatigue of deformable materials, and to examine the range of validity of the polymerization and crosslinking mechanisms discussed above, work was begun to study in detail the effect of corona induced fields on the elastic properties of room temperature vulcanized (RTV) rubbers. General Electric RTV 619 was selected for study because of the ease with which it deformed compared to other RTV rubbers, and because of its paste-like character which promised both greater surface movement and greater susceptibility to covalent-band ciosure.

The devices were fabricated in a manner similar to those which employed the silicon elastomer (Fig. 9) except that RTV 619 was used as the deformable media. An analysis was done to learn whether the material fatigue occurred at the onset of deformation, long after deformation had occurred, or while the material was deforming. The procedure was as follows: using the experimental arrangement of Fig. 10, two beams were made to interfere on the RTV surface; during exposure the corona discharge was turned on for several seconds, and then turned off.

b. Experimental data. A permanent hologram was found to be recorded in the RTV indicating that one cycle of corona discharge had permanently fatigued the material, presumably through electric field/corona induced polymerization and crosslinking. Figure 12 is a 1X photograph showing the readout from the hologram in which the eighth order is seen to be visible. Because of the comparatively high intensity of the lower orders, Fig. 12 is a superposition of a 0-2, 3-5 and 6-8 order exposure in which the higher orders were sequentially blocked using a piece of cardboard. The intensity of the higher order diffracted beams as well as the light power incident on the sample (Beam A) was measured using a photodiode type detector circuit. In these measurements, the photodiode was placed between the sample and the viewing screen after the hologram had been permanently stored in the deformable media. Photographs were later taken of the permanently fatigued surface. Figures 13A,B show a 192X and 960X, respectively, enlargement of the surface detail of the RTV 619 from which the deformation wavelength was measured to be ~6.8 μm, i.e., $k \sim 0.92 \times 10^6$.

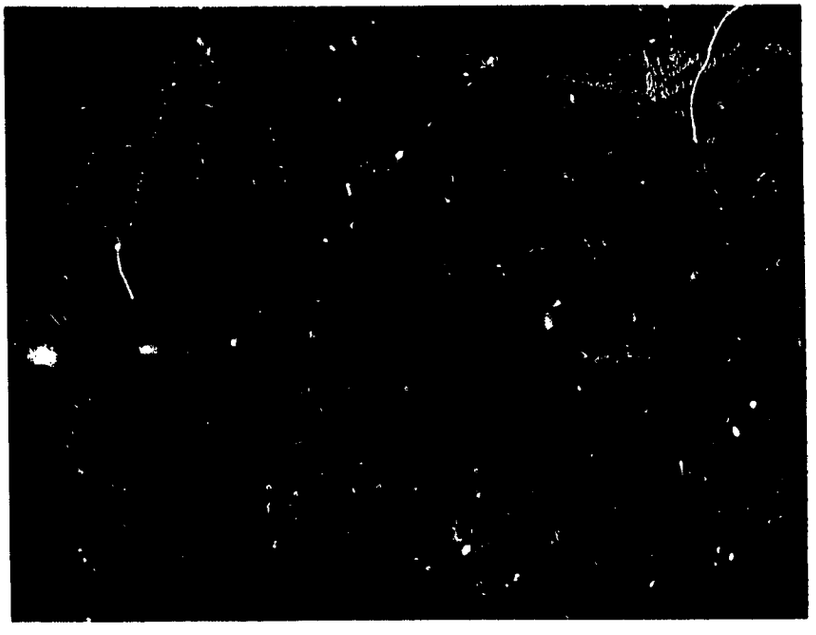

Figure 12. Differential orders zero through eight (multiple exposure).

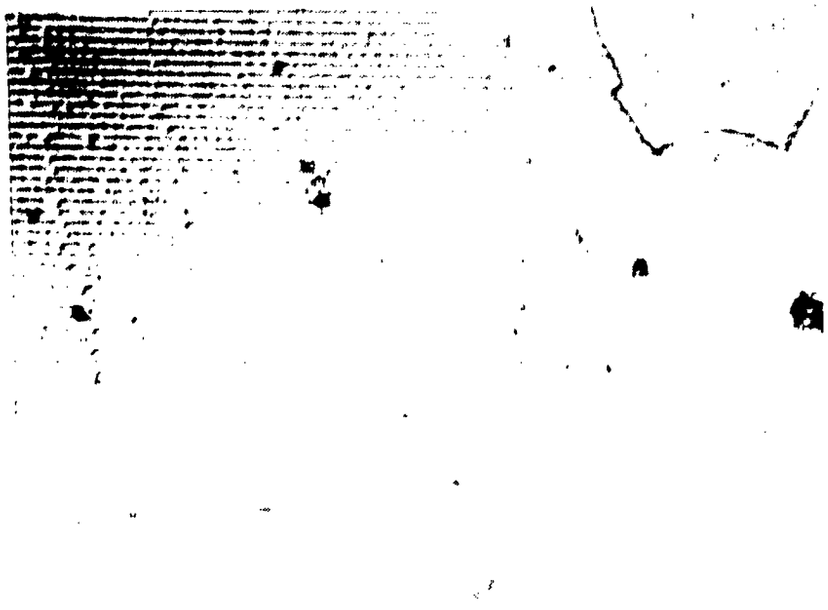

(192X)

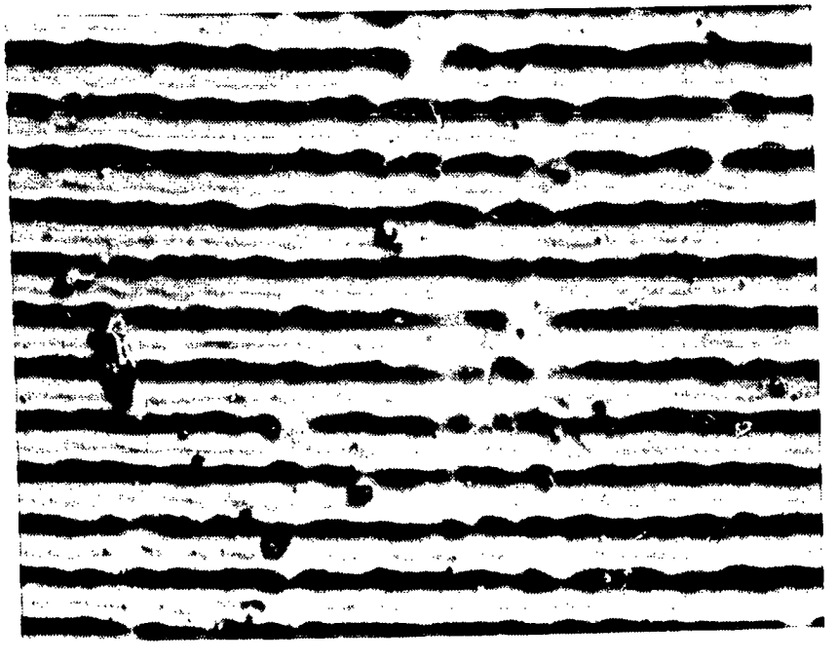

(960X)

Figure 13. Grating permanently stored in GE RTV 619.

The fatigue in the RTV material can be shown to occur while the film is deforming at a depth approximately equal to one-half of the film thickness. Since no heat is involved in the process, the polymerization, and crosslinking ostensibly occur in response to electrostatic energy supplied by the corona discharge.

I. Conclusions

A fundamental conclusion of this work is that partially polymerized crosslinked polymers are unsuitable for use as a deformable holographic storage material, and that a fatigue-free deformable material must consist either of a completely polymerized and crosslinked polymer deformable at practical temperatures, or a material wherein sufficient molecular integrity exists to preclude further unit volume free energy reductions through molecular restructuring during repeated phase changes.

IV. MICROCRYSTALLINE WAX

A. Introduction

A survey of materials with fully polymerized and crosslinked structures was initiated and conducted concurrent with the work described above. As a result of the survey, it was concluded that polymers with such structures are generally nondeformable at reasonable temperatures and magnitudes of electrostatic force, in addition, they usually necessitate the use of solvents not compatible with conventional organic (sensitive) photoconductors.

During the course of the materials investigation into fully polymerized and crosslinked polymers, a linear, low-molecular-weight hydrocarbon-polymer class of organic materials was uncovered which promised molecular structural integrity during thermal phase changes. This class of materials consisted of complex mixtures of normal paraffinic, isoparaffinic, and naphtheric solid hydrocarbons, and is commonly referred to in industry as microcrystalline wax.

B. Structure

1. Molecular stability. — Unlike paraffin wax which changes in molecular composition upon repeated liquification and solidification, and which is composed almost entirely of hydrocarbons of the normal-paraffin series, microcrystalline wax, in addition to the straight chain components, contains naphthenes and isoparaffins with properties that differ greatly from those of the normal-paraffin series. In this respect the microcrystalline waxes are unique; for example, intermediate waxes in addition to straight chain components also contain naphthenes and isoparaffins, but unlike microcrystalline wax the physical properties of the latter compounds differ only moderately from the normal-paraffin series.

Although paraffin, intermediate and microcrystalline waxes can be found with identical melting points, their physical properties are quite different due to variations in chemical composition. The hydrocarbons of which microcrystalline wax is composed appear to double-over on themselves and self-interact in a fashion which produces a lower overall energy per molecule. This reduced energy state apparently imparts molecular stability during repeated liquification and solidification, and acts to produce a high degree of plasticity within the material. The molecule appears to be further stablized because of isolated, branched-chain and saturated, cyclic-ring structures which seem to attach themselves at points of imperfection along the straight hydrocarbon chain, as well as near the ends of the chain where straight-chain molecular attachments (and therefore changes in physical properties) most frequently occur.

2. Physical properties. — The microcrystalline wax usually is found to contain an irregular and small crystalline structure, in sharp contrast to the large, well-defined crystals most often seen in paraffin wax; in addition to a comparatively high molecular weight, ~600-700, microcrystalline

waxes also have a higher boiling point and refractive index. Although its melting point is also higher, thin film coatings have been found to adequately soften at about 42°C, a temperature which is quite reasonable from a holographic memory systems viewpoint.

Other characteristics of the microcrystalline wax are its approximately uniform molecular composition, thereby yielding a comparatively narrow ~2-3° transition temperature, a dielectric constant of ~2.8 comparable to the PVK photoconductor, a reasonable dielectric breakdown strength $\sim 10^7$ V/m, a surface resistivity adequate for holographic storage $\sim 10^{15}$ ohms/square, and a viscosity ~5 centipoise, more than sufficient to accommodate typical electrostatic forces.

C. Device Configuration

1. Fabrication sequence. — Devices containing microcrystalline wax as the deformable media were fabricated using 2.5 cm by 2.5 cm, 2.5 cm by 5 cm, and 5 cm by 5 cm substrates. The different substrate sizes were useful in the many different kinds of experiments which were performed. The smaller substrates were employed in photoemission experiments where it was necessary to seal the samples in high-vacuum tubes. The large substrates were convenient for both process development for sample fabrication and evaluation of holographic storage over large areas. The intermediate (2.5 cm by 5 cm) substrates were employed for special-purpose experiments including definition of operating parameters such as temperature, heat-pulse duration, charge rate, etc.

Both tin oxide (TIC) and indium oxide (InO) were used as the transparent electrode. Regardless of substrate size, the general deposition sequence was as follows: glass substrate, transparent electrode, barrier layer (optional), photoconductor, and microcrystalline wax. This device structure is illustrated in Fig. 14.

2. Chemical barrier. — The structure shows a barrier layer, which was employed to prevent a chemical reaction between the photoconductor and the wax during experiments in which a constant thermal bias was applied to the wax. This constant thermal bias was accomplished by passing a dc current through the transparent electrode, which served to maintain the temperature of the wax in these experiments just below its softening or melting point. However, no such chemical reaction occurred if the heat was rapidly applied to the wax in the absence of thermal bias, i.e., if the transparent electrode was pulsed over time durations of the order of milliseconds with the wax normally maintained at ambient (~25°C) temperature. For these reasons, the barrier was usually employed in experiments where a thermal bias was present.

3. Fabrication recipe. — A recipe which was found to be satisfactory for general-purpose sample fabricatio provides for dissolving between 0.8 g to 1.2 g of microcrystalline wax (depending upon the desired thickness) in 160 cc of N-hexane, and heating the solution to a temperature of about 60°-65°C. The TIC- or InO-coated glass substrate with photoconductor layer is then immersed in the wax solution and withdrawn at a rate of 5 cm per second. When the protective barrier is desired, it is applied as follows: between 0.15 and 0.30 g (depending upon the desired thickness) of

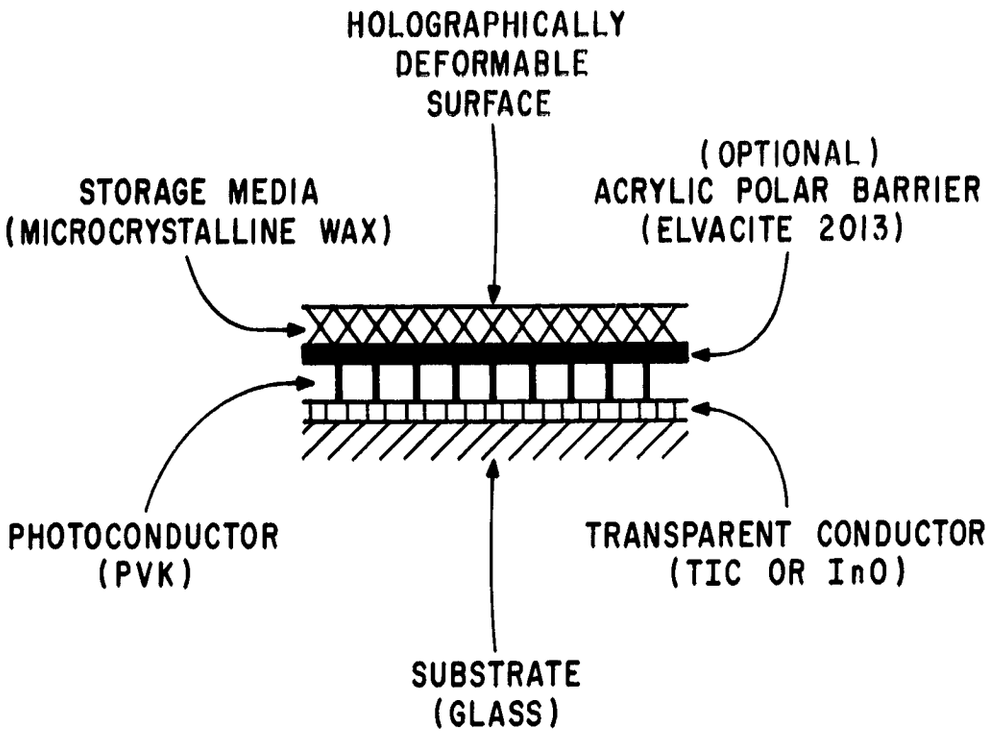

Figure 14. Microcrystalline wax device structure.

Dupont Elvacite 2013 is dissolved in 5 cc of acetone at a temperature of about 60°C; 50 cc of ethyl alcohol whose temperature also is about 60°C is then slowly added (drop by drop) to the 5 cc acetone solution; the substrate (TIC- or InO-coated glass and photoconductor) is then submerged in the composite acetone-ethyl-alcohol solution and withdrawn at a rate of between 2.5 and 5.0 cm per second (depending on the desired thickness). A very-high-quality protective coating chemical barrier is produced on the photoconductor, which does not contain any discernible defects. It is found that only the #2013 resin is practical. Lower-molecular-weight resins do not dissolve in usable solvents, and higher-molecular-weight resins have incomplete molecular saturation which detrimentally and irreversibly polymerizes and crosslinks to produce non-erasable holograms. This occurs because of the same fatigue mechanisms discussed earlier; only in this instance it occurs in the barrier layer with Elvacite resins of higher molecular weight than Dupont #2013.

Although the fabrication recipe described above has been found satisfactory, additional process development work directed toward improvement of surface roughness is highly desirable. The surface of the microcrystalline wax as presently deposited contains many microscopic imperfections which serve to scatter incident laser light. Figure 15 is a photograph of the readout of a 16 × 16 checkerboard pattern from a hologram stored in microcrystalline wax, in which the scattered light is easily visible. Several techniques exist whereby surface roughness could be substantially improved, and the random scattering greatly reduced.

Figure 15. 16 × 16 checkerboard readout with scattered light.

D. Surface Charge

1. Corona discharge. — Experiments were performed and measurements taken which employed two different methods for supplying charge to the wax surface. The first technique used a corona discharge device, while the second method employed a unique, space-charge-neutralized, demountable, glow-discharge chamber. The corona-discharge device consisted of a simple corona-discharge needle, which was separated from the sample by about 0.6 cm. Typically, a voltage of about 5000 V placed across the needle and the transparent electrode of the sample was adequate to produce a corona discharge of about 5-10 μA.

2. Corona properties. — Even though the distance between the needle point and the deformable wax surface was controlled, and the corona current monitored, the corona-charging method with a single, unshielded needle contains characteristics which are undesirable. For example, the rate of charge and electric field intensity across the deformable surface tend to be nonuniform. In addition, dielectric breakdown occurs between the wax surface and the transparent electrode unless a control grid is employed and placed with about 25 μm of the surface. Unequal mechanical forces also exist along the surface due to bombardment by ionized air molecules within the nonuniform corona-discharge stream which can cause adverse effects; and thermal instability sometimes occurs because of interaction between room air currents and the cooling effect associated with the corona discharge. Although many of these deficiencies can be circumvented through the use of techniques discussed in a later section, another approach to the problem was found which proved useful for the acquisition of data over a wide range of experimental conditions.

3. Demountable glow discharge chamber. – A unique, demountable chamber was developed, in which the surface potential of the wax was controlled by controlling the potential energy of the inert gas molecules within a space-charge neutralized glow discharge. The chamber is illustrated in Fig. 16, and was maintained at reduced (~ 1/2 mm Hg) pressure. The inert atmosphere provided

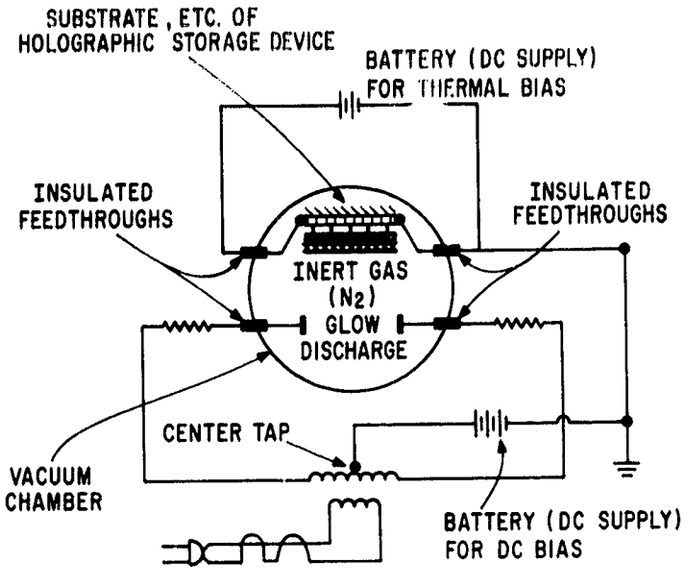

Figure 16. Space charge neutralized demountable glow chamber.

an environment free of ambient fluctuations. This latter feature proved to be of great value, and in several experiments permitted the practical maintenance of a stable temperature bias on the holographic wax storage media.

4. Chamber properties. – A residual bias was found to exist in the chamber, which was reduced through use of a lower-molecular-weight gas (argon). Improvements in control of the surface potential were obtained by increasing the frequency of discharge excitation from 60 Hz to 30 kHz. Confinement of the ac electric fields to regions removed from the deformable wax surface was achieved through design and construction of an all glass demountable tube. Figure 17 is a photograph of one such design used in earlier work with smaller substrate samples.

5. Chamber design. – The design of Fig. 17 reflects a major improvement over earlier versions in that all contaminants including glyptal have been eliminated from the chamber. This was made possible by having all electrical connections to the sample external to the tube, and installing the sample in a manner whereby only the microcrystalline deformable surface is exposed to the space-charge neutralized discharge. This method of sample installation is illustrated in Fig. 18. As shown in the figure, the coil supplies the ac voltage necessary to maintain the ionized state of the inert gas, whereas the dc battery via the center-tap on the coil is used to control the potential at the wax surface via control of the potential energy of the ionized molecules referenced to the transparent electrode.

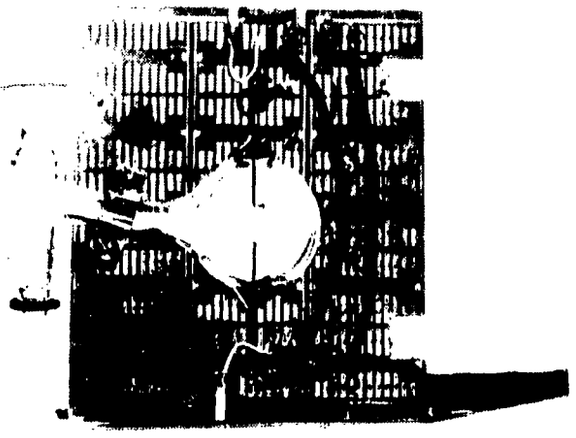

Figure 17. Photograph of all glass demountable glow chamber.

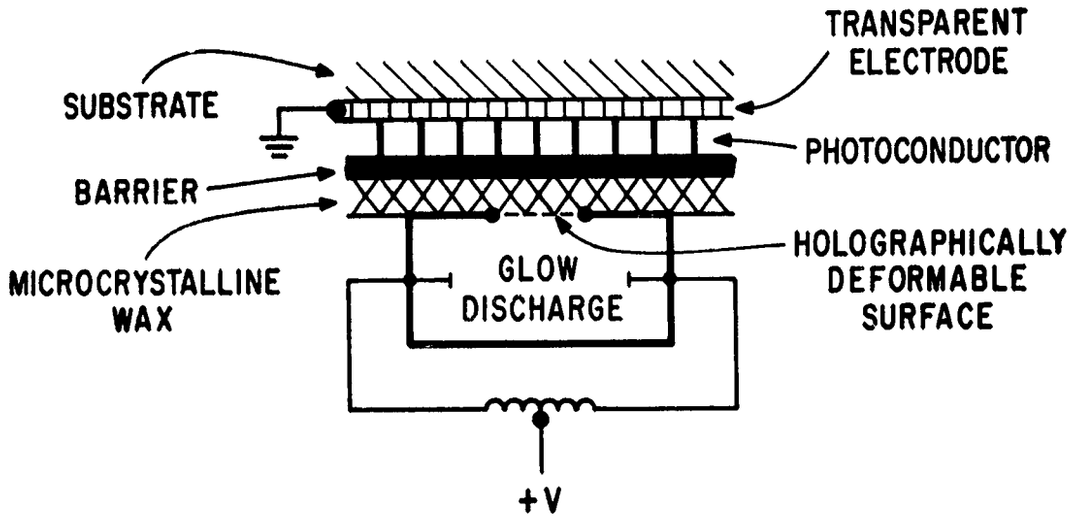

Figure 18. Sample installation on glow chamber.

E. Experimental Results

1. Diffracted orders. — Many experiments were conducted using either the corona-discharge devices, or space-charge neutralized chambers to provide charge to the wax surface. As a result of these experiments, the fabrication recipe discussed earlier was found to be satisfactory and wax thickness of the order of 1 μm were shown to be adequate. Microcrystalline wax films were fabricated, and two-beam holograms routinely recorded which exhibited ninth-order diffracted

beams. The experimental arrangement necessary to record such holograms is shown in Fig. 19. The diffracted orders from a typical 2.5-cm by 5.0-cm sample are shown in Fig. 20A; a longer exposure has been made in Fig. 20B to show the actual path of the diffracted laser light.

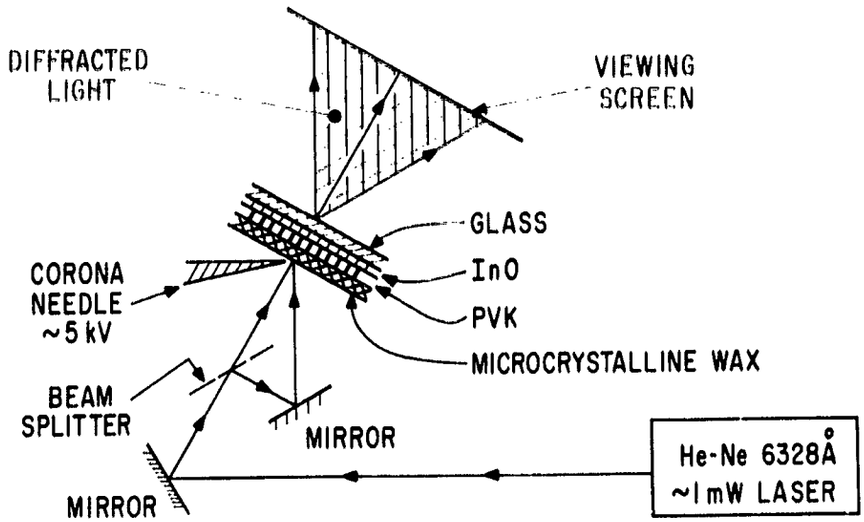

Figure 19. Experimental arrangement for microcrystalline wax hologram recording.

2. Thermal bias above threshold. — Although numerous holograms were recorded and erased using corona-discharge devices, the use of the space-charge neutralized chamber permitted holographic read/write cycles under a variety of conditions not otherwise possible. In one investigation, a constant-thermal bias was maintained above the temperature of wax-surface deformation and the surface potential was controlled through use of a dc-voltage bias applied to the inert gas discharge. Holograms, which were observed with both reference and object beams simultaneously present, disappeared upon removal of either one of the two beams; the holograms also were made to disappear upon removal of the dc-discharge bias or the ac glow discharge excitation voltage.

3. Thermal bias instrumentation. — In other work a constant power unit was designed and constructed which multiplied the heater voltage and current applied to the transparent electrode, and maintained this product equal to some constant preset level. The constant-power unit had provision for a dynamic mode in which it was electronically disabled over time periods ranging from tens of microseconds to tens of milliseconds, during which narrow-heat pulses were superimposed upon the constant-thermal bias to yield controlled narrow-temperature excursions within the deformable wax media. This and other instrumentation used in the experiments are shown in Fig. 21.

A

DIFFRACTED ORDERS

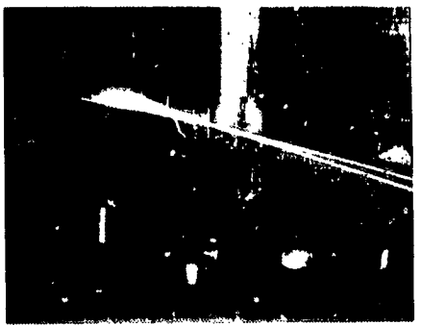

B

LASER LIGHT PATH

Figure 20. Diffracted orders and laser light path.

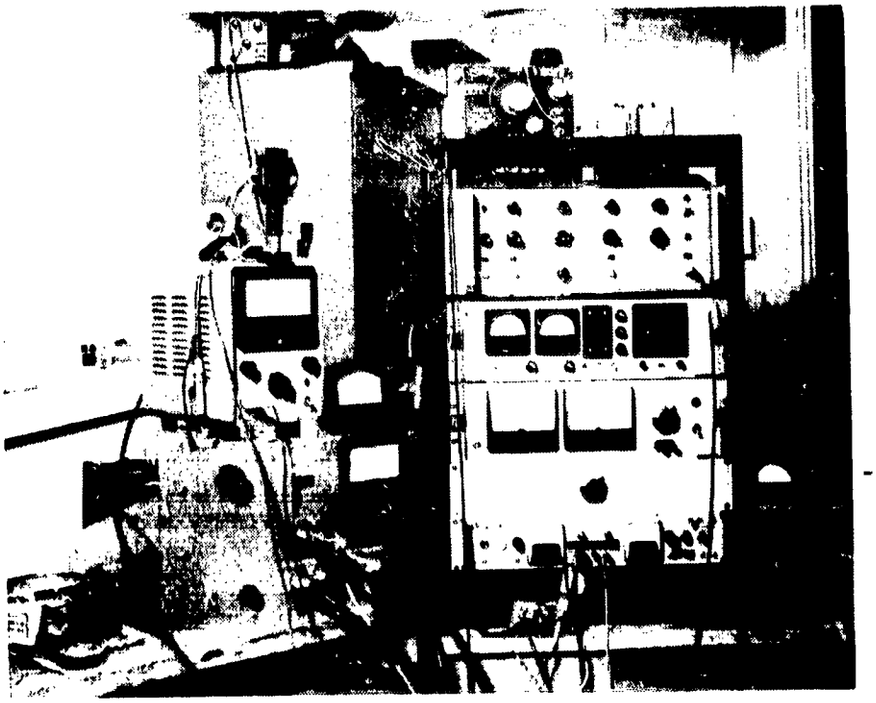

Figure 21. Photograph of instrumentation.

4. Thermal bias below threshold. In one experiment, the microcrystalline wax was maintained at a constant-thermal bias just beneath its melting temperature, and a current (heat) pulse applied to the transparent electrode over an interval of 10 μsec. Under these conditions, a hologram which had been previously stored in the wax was observed not to erase. The absence of erasure of the previously stored hologram over this time period, and at the level of applied power (up to 1.5 A into 100 ohms), indicated that surface restoration of the microcrystalline wax occurs over intervals of time longer than 10 μsec. This result was substantiated in later work in which measurements were taken of the relationship between the heat-pulse amplitude and heat-pulse duration necessary to write and erase holograms in the microcrystalline wax media.

5. Absence of fatigue. — Using a corona-discharge device and the experimental arrangement of Fig. 19, experiments were performed uninterrupted over a 3-day period in order to evaluate what fatigue, if any, would appear in the microcrystalline wax. A corona discharge was established and maintained continuously over this period during which two-beam holograms were successfully written and erased using repetitive heat pulses of 5-msec duration spaced several seconds apart. Well over 7000 read/write cycles were performed on the microcrystalline wax storage medium with no discernible fatigue. This experiment confirmed our expectations, and provided additional support of the conclusions in regard to material-fatigue mechanisms discussed earlier.

Unlike the room-temperature vulcanized rubbers, microcrystalline wax may be regarded as incompressible in the regime over which holographic deformation occurs. In addition, surface rather than elastic energies interplay with the electrostatic energy to yield a surface contour for which both surface and electrostatic energies are a minimum. The condition for a stable-surface deformation is shown in Appendix A to be

$$W_s > \frac{d}{4s_o}\,\epsilon\,V^2 \tag{7}$$

where W_s is the surface energy, d the period of surface deformation, s_o the wax thickness, and V the potential along the wax surface. It is shown in Appendix A that the onset of frost in the wax occurs with periods longer than d and that

$$d > \frac{\pi}{\sigma_o}\left(2\epsilon_1 s_o T\right)^{1/2} \tag{8a}$$

for $k s_o << 1$

and

$$d > \frac{4\pi\epsilon_1}{3\sigma_o^2}\,T \tag{8b}$$

for $k s_o >> 1$

where σ_0 is the surface charge density, and T the surface energy per unit area. Thus, for large values of wax thickness s_0, the frost spectrum is independent of the thickness, while for small values of thickness, the limiting frost wavelength decreases with the square root of s_0. Defining the dielectric breakdown strength of the wax as $E_B = V_0/s_0$, Appendix A gives the stability criterion for recording holograms in the wax [Eq. (71)] in terms of the per unit area surface energy of the wax as

$$T = 2\epsilon s_0 \left(\frac{E_B}{k s_1} \right)^2 \tag{9}$$

Taking $s_0 = 1\mu m$, $k s_1 = 1$, and $E_B = 10^7$ V/m, and $T = 4.10^{-2}$ J/m^2 for microcrystalline wax, the stability criterion imposed by Eq. (9) is satisfied by about an order of magnitude. However, as the temperature is increased above the softening point, an abrupt nonlinear decrease in the surface energy T occurs, and the constraint imposed by Eq. (9) is no longer anticipated to hold.

6. Diffraction efficiency versus heat-pulse amplitude. In order to evaluate the stability criterion, as well as possible charge loss due to increases in electrical conductivity of the wax with temperature, single pulses of heat were applied to the wax by pulsing the transparent electrode with voltage pulses of controlled amplitude. Measurements were taken of the intensity of the first-order diffracted beam as a function of heat-pulse voltage amplitude for each of several heat-pulse widths ranging in duration from 6 to 10 msec. Figure 22 is a plot of the data, where for a given width of heat-pulse duration, the diffraction efficiency is seen to first increase with increasing heat-pulse voltage, reach a maximum value, and then decrease as the temperature is increased further.

7. Diffraction loss versus surface energy. — The initial increase in first-order diffracted output is caused by the reduction in viscosity (surface energy) as the wax becomes softer. The decrease in output efficiency beyond a certain value in heat-pulse voltage may be attributed to either or both of two effects: (1) a reduction in surface charge density (σ_0) due to an increase in electrical conductivity with temperature thereby reducing the net surface forces, and/or (2) a reduction in surface energy below a value adequate to satisfy the criterion imposed by Eq. (9). Since the measurements were conducted using a corona-discharge device of copious emission ($\sim 2\,\mu$A/mm), and since the decrease in output efficiency is seen in Fig. 22 to be quite abrupt over a comparatively narrow increase in heat-pulse voltage (~ 2 %), it seems doubtful that a sharp increase in charge loss occurred in such a narrow temperature interval above and beyond that supplied by the corona discharge. This conclusion is also supported by other work in which independent measurements of the electrical conductivity of the wax with temperature were made showing a maximum increase in conductivity by a factor of five over a temperature range of about 40°C. The conclusion therefore is that the abrupt decrease in the first-order diffracted intensity with heat-pulse voltage, is most likely due to the nonlinear decrease with temperature of the surface energy of the wax to a value insufficient to satisfy a stable surface contour [Eq. (9)].

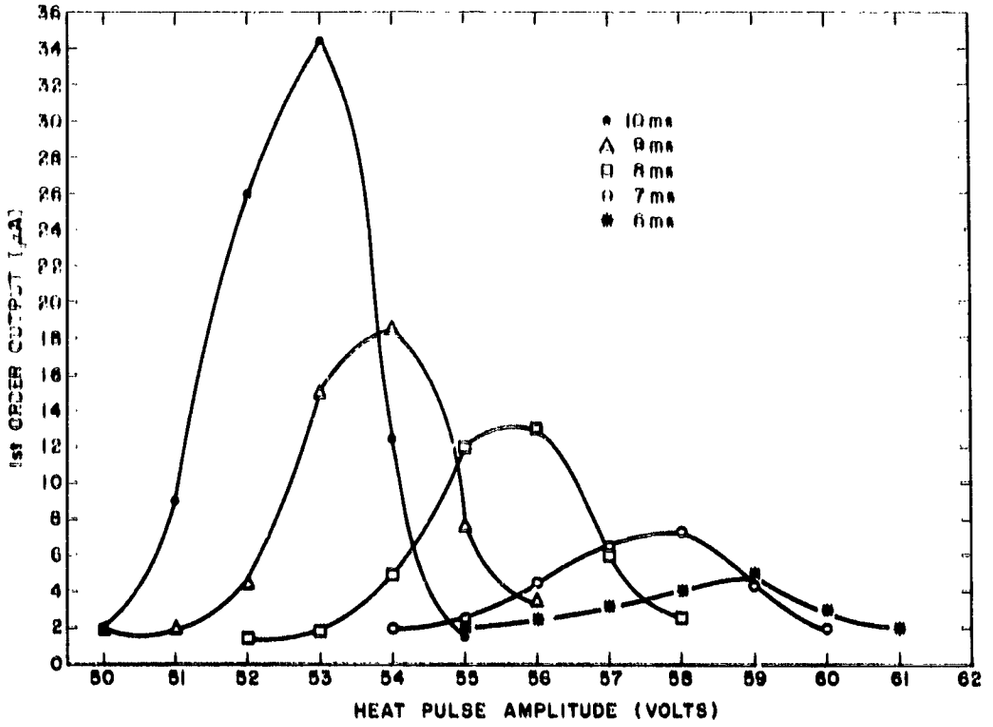

Figure 22. First order output versus heat pulse amplitude for microcrystalline wax.

8. Response time. — Of interest in the data is the decrease in diffraction-output efficiency with decreasing duration of the heat pulse. Analysis of the heat flow to and from the wax discussed in a later paragraph indicates that the maximum output efficiencies shown in Fig. 22 appear to occur at somewhat lower temperatures as the heat-pulse duration shortened. This means that the diffracted-output efficiency for the same temperature of wax is lower for narrower heat pulses. One explanation for this phenomenon is that the duration of the heat pulse is comparable to, and approaching, the inherent response time of the wax. Experiments done at heat-pulse widths down to 0.5 msec show the response time of the wax to be of the order of 2 msec.

9. Surface energy versus chemical additive. — The speed with which the wax responds to the electrostatic surface forces depends upon viscosity and surface energy. In order to evaluate this factor in greater detail, work was initiated to find a material which when added to the microcrystalline wax would produce a substantial increase in the surface energy near the softening point of the wax. Dupont Elvax 310 was selected as the additive and samples were fabricated and evaluated. The results from these experiments are shown in Fig. 23. Note that although the initial first-order output intensity for a heat-pulse duration of 10 msec appears smaller than that of Fig. 22, they are of comparable magnitude due to the change in scale. The data shows a significant improvement in response time of the microcrystalline wax with the diffracted-output efficiency increasing with decreasing duration of heat-pulse width. The data indicates the response

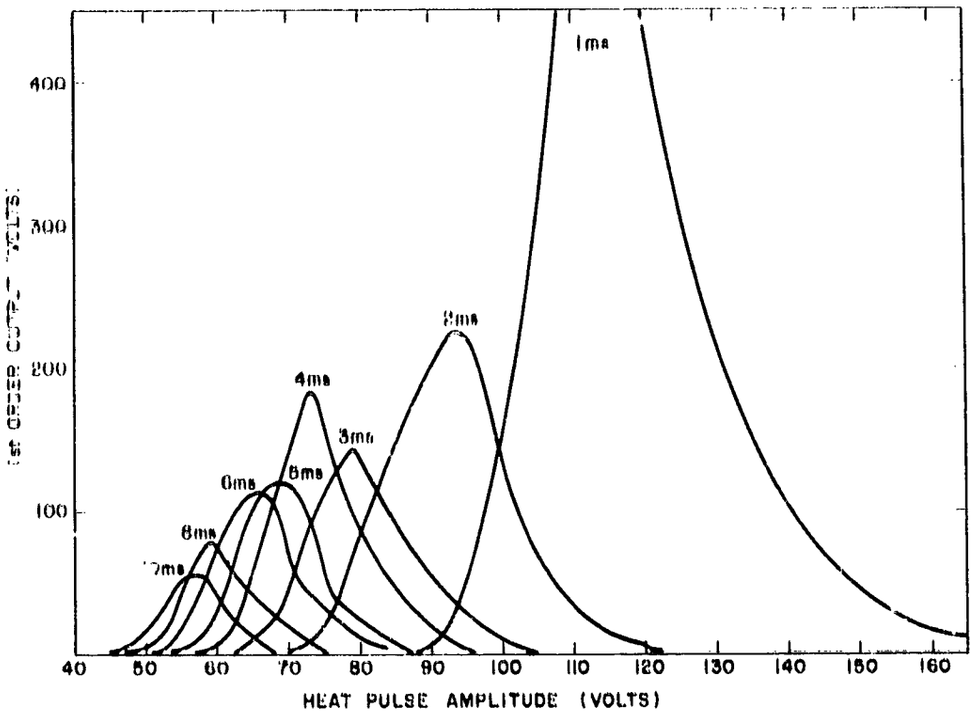

Figure 23. First order output versus heat pulse amplitude for microcrystalline wax with additive.

time to be considerably lower than 1 msec. However, additional tests revealed that after many repetitive cycles, the additive produced material fatigue due to corona discharge, induced polymerization and crosslinking. This was traced to incomplete molecular saturation of the Elvax additive.

10. Heat-pulse amplitude versus heat-pulse duration. – A thermal analysis was done on the heat-pulse amplitude and duration necessary to produce a given temperature in the wax coating. The analysis is given in Appendix B where it is shown that, to a good approximation, the thermal energy (W_t) necessary to produce a given temperature is related to the time duration (τ) over which it is applied as

$$W_t^2 = C'\tau \tag{10}$$

where C' is some constant. Since the power in the heat pulse is simply the square of the voltage (V) divided by the resistance (R) of the transparent electrode

$$W_t = \frac{V^2\tau}{R} \tag{11}$$

Equations (10), (11) therefore give

$$V^4\tau = \text{constant} \equiv C'R^2 \tag{12}$$

Measurements were taken to experimentally determine the relationship of the heat-pulse amplitude and duration necessary to write and erase holograms in the microcrystalline wax. The data is summarized in Figs. 24 and 25, which are log-log plots of write and erase data, respectively. The

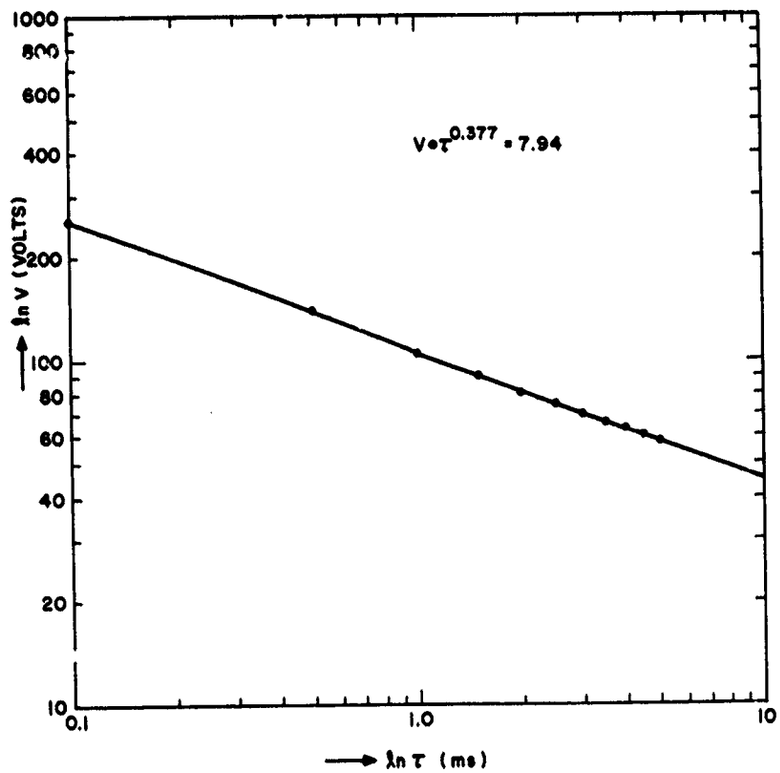

Figure 24. Plot of heat pulse write amplitude versus pulse width.

write data consists of the measured heat-pulse voltage and duration necessary to write a hologram in the wax storage media; the holograms were erased using a preset-erase heat pulse. The erase data consists of similar measurements in which the holograms were written using a preset write pulse. The data of Fig. 25 shows excellent correlation with Eq. (12), i.e., $V_\tau^{0.27}$ = constant. The slight departure from the fourth-power root evident in Fig. 24 is not surprising since both the charge leakage and surface-energy effects discussed earlier also play a role.

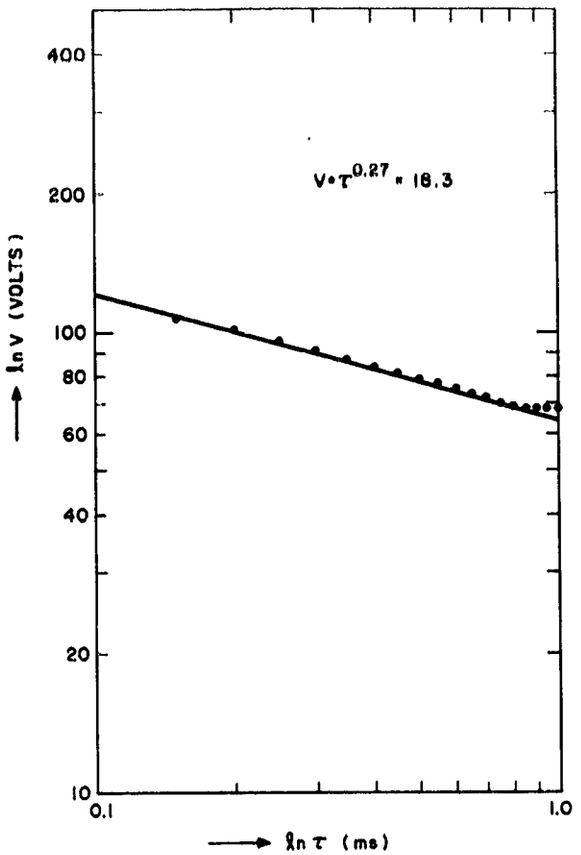

Figure 25. Plot of heat pulse erase amplitude versus pulse width.

F. Microcrystalline Wax Summary

A class of organic materials consisting of complex mixtures of normal paraffinic, isoparaffinic and naphthenic solid hydrocarbons has been found which exhibits no discernable molecular structural change during repeated liquification and solidification. Commonly referred to in industry as microcrystalline wax, holograms were repetitively recorded and erased at least 7000 times under continuous corona-discharge exposure with no apparent fatigue effects. The unique physical properties of the material derive from: (1) widely differing compositional properties of the napthenes and isoparfine from those of the normal-paraffin series, and (2) a double-over self-interacting hydrocarbon chain which ostensibly imparts an overall lower energy and stability to the molecular system, and plasticity to the material as a whole. Other desirable properties include a narrow ~ 2-3° transition interval, adequate surface energy over this temperature range for stable surface deformation, a dielectric constant comparable to the PVK photoconductor, good dielectric-breakdown strength, adequate surface resistivity, low viscosity near the softening temperature, good response time, write sensitivity and readout efficiency, photoconductor solvent compatibility, and ease of thin-film fabrication.

V. HOLOGRAPHIC STORAGE TUBES

A. Introduction

The successful development of the microcrystalline wax as a holographic-storage medium useful at modest temperatures (~40-45°C) and energies (~10^{-7} J/mm) resulted in its application for use in holographic-recording tubes. Tubes of various configurations were designed, constructed and evaluated in which electron heating and photoconductive and photoemissive mechanisms were employed in conjunction with the wax storage medium.

In one instance, staybelite was used as a vehicle to evaluate a demountable vacuum chamber using a thermionic emitter for electron heating. The use of staybelite as a storage material is presented in Vol. I of this report, and is therefore not discussed here. Although the material exhibits fatigue after several hundred write/erase cycles, apparently due to surface oxidation in conjunction with bulk fatigue associated with impurities, its use in both the optical memory system and thermionic and photoemission holographic storage tubes proved of value in system and tube evaluation. Photoemission mechanisms employed both for heat addressing, and as a means to charge the deformable surface were used in tubes of various designs in which microcrystalline wax was used as the storage medium. Complex styrene was successfully used in these tubes as a barrier to isolate the wax from the high vacuum [$\geq 10^{-5}$ μm ($\geq 10^{-8}$ torr)]. The styrene was sufficiently thin however (~80 nm) to allow surface deformation of the wax. The various holographic-recording tubes are discussed below, including a unique corona-discharge chamber in which holograms were successfully written and erased over a 2-cm by 2-cm area. This chamber together with the microcrystalline-wax storage medium proved to be the most successful of all the methods employed. Heat addressing was accomplished using about 80 mW from an argon laser.

B. Thermoplastic Recording via an Electron Beam in a Demountable System

To examine the behavior of thermoplastics under electron-beam bombardment, a demountable vacuum system, shown in Fig. 26, was built. This system incorporated an electron gun, deflection yokes, vacuum gauges, and a viewing window. The targets tested were thin (0.1-10 μm) films of thermoplastic on InO-coated glass substrates. The thermoplastics used were staybelite ester 10 and a commercial polystyrene PS-2. Several experiments were made with a photoconductive layer under the thermoplastic layer in an attempt to record holograms, but the mechanical vibrations due to the vacuum pumps were too severe to achieve success.

By using the electron beam to charge the plastic, and resistance heating the InO-coated substrate, frost patterns could be formed and erased. A magnified view of one such frost pattern is shown in Fig. 27. It is similar to frost patterns formed by conventional corona charging in normal thermoplastic recording. The charge needed to form the frost was approximately 10^{-5} C/m^2. The accelerating voltage had to be kept below 3×10^3 V for efficient frost formation. Voltages higher

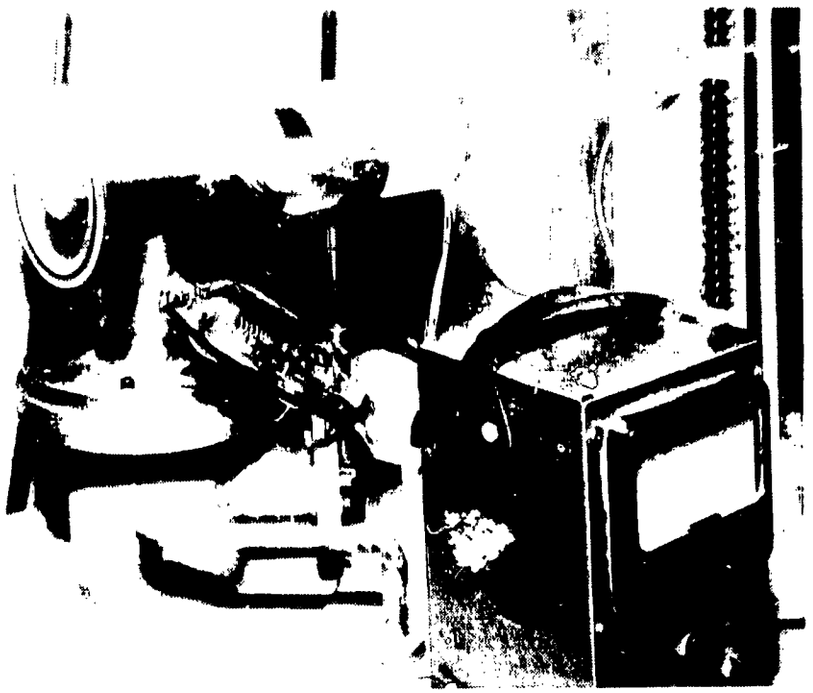

Figure 26. Photograph of demountable vacuum system.

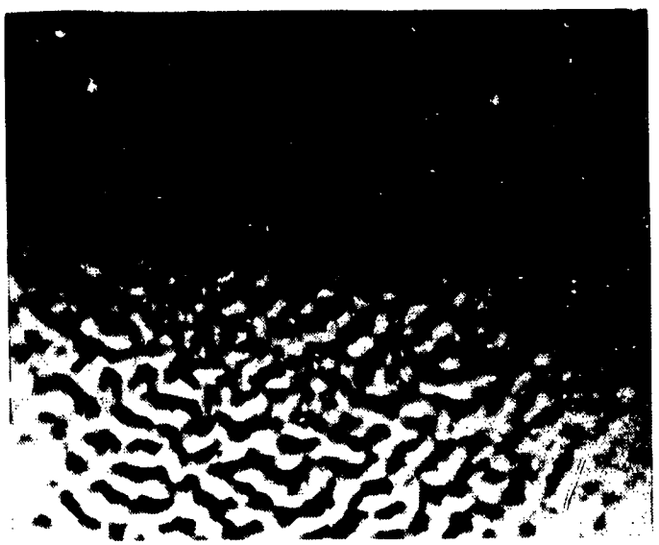

Figure 27. Frost pattern due to electron beam charging.

than this led to electron penetration too far below the surface of the plastic to be useful in deforming the film. It is noteworthy that the penetration depth of electrons is given by $h = 0.02\ V^2$, where h is the penetration depth in μm and V is the accelerating voltage in kV. For acceleration voltages less than 3×10^3 V the penetration depth is less than 100 nm, while, for example, an acceleration voltage of 10^4 V would imply penetration depths of greater than 1 μm – greater than the film thickness in some experiments.

The pressure in the system was constantly monitored and it was found that in the initial cycles, the pressure increased by several orders of magnitude [e.g. from 10^{-3} to 10^{-1} μm (10^{-6} to 10^{-4} torr)]. After several thermal cycles, the pressure variations decreased. The pressure variations are probably caused by material evolved from the plastic during heating. Although the amount of material evolved could be limited by preheating the target, the implication of this experiment is that the problem of maintaining a vacuum in a sealed system using this material would be severe.

The temperature of the target was monitored by means of a thermocouple. It was found that after a heat time of 1 or 2 seconds it took several minutes before the target cooled to its initial temperature. This is in agreement with the analysis given in Appendix B.

C. Electron-Image Tube

One of the methods examined to obviate the need for redundant selection of the page on the storage plane (that is, once by light and once by heat) involved the arrangement and structure schematically shown in Fig. 28.

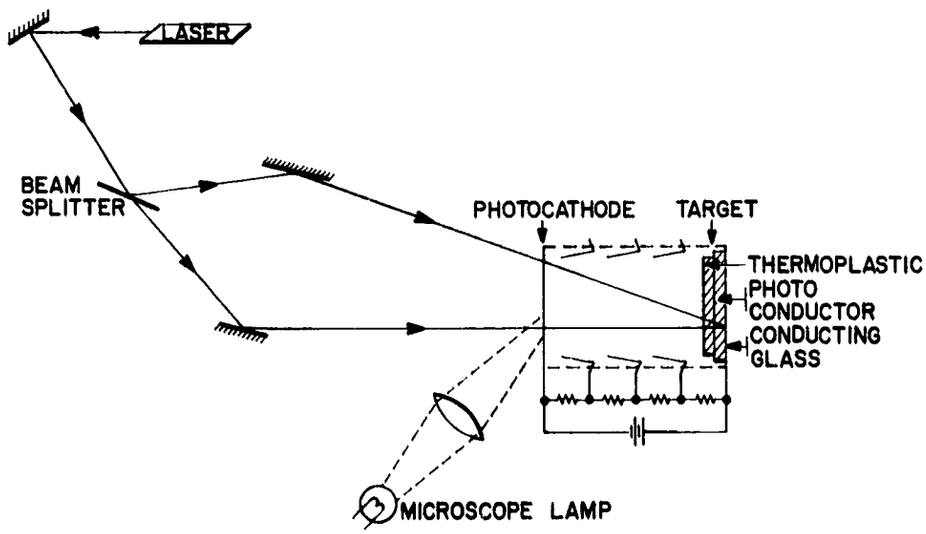

Figure 28. Experimental arrangement using electron-image tube.

The storage plane was a conventional, thermoplastic-photoconductor arrangement and the recording process involved the usual steps of charge-expose-charge and heat. In this experiment, however, both charging and heating were done with an electron beam generated by photoemission from a photocathode.

The essential structure is that of a proximity-focussed electron-image tube, with the target being the thermoplastic-photoconductor conductive-substrate arrangement. The tube is positioned so that the reference beam is coaxial with the tube, and thus parallel to the electric field between the target and photocathode. When the reference beam is incident on the target (and therefore also on the photocathode), electrons are generated that are accelerated to and land at the same location on the target. At low accelerating voltage (of the order of 500 V) these electrons do not penetrate much below the surface of the thermoplastic. This structure allows a simple means to selectively charge a particular location on the storage plane. To ensure that the absorption of the electrons does not cause heating, the accelerating voltage is kept low (< 500 V) and the current density is limited by using an attenuated reference beam. To heat the thermoplastic, which is necessary to develop the hologram, the accelerating voltage is increased (< 2000 V) and the intensity of the reference beam is increased, which leads to a corresponding increase on the electron beam intensity.

Several experiments were performed to investigate the feasibility of this structure. The targets used consisted of a 600-nm thermoplastic (staybelite ester 10) layer over a 2-μm photoconductor (a poly-N-vinyl carbazole doped with trinitro-fleurenone) layer which was deposited on an InO-covered glass substrate. The size of the substrate was 2.5 cm by 2.5 cm. The target was mounted to a window of one of the standard RCA image tubes, and the InO was connected to the end ring of the image tube.

The tube was sealed and the window opposite the target was activated with standard cesium-antimony layers to form a S-11 photocathode. The tube was baked at 75°C for about 24 hours to remove some of the contaminants. This low bake-out temperature was used to avoid possible damage to the staybelite-thermoplastic layer.

The photoelectric sensitivity of the photocathode was measured to be 2-5 mA/W, i.e., about one-tenth of that normally obtained in this type of image tube. The decrease in sensitivity is due both to inadequate bake-out and impurities introduced by the plastics.

Because of the low sensitivity, light from a microscope lamp was imaged at the photocathode in the initial device feasibility tests, thereby avoiding switching of the reference beam intensity. The auxiliary source was imaged at the same location on the photocathode as the reference beam and at an angle, so as to minimize its effect on the photoconductor.

Holograms were stored in the device by simultaneously applying light and charge while heating the film. A low voltage (< 500 V) was first applied to the tube; the voltage was then

quickly increased to the order of several thousand volts. During this time, the object and refer ence beams and the auxiliary lamp were kept constant.

These experiments were repeated numerous times with a number of different tubes. The results were repeatable. The successful recording of holograms in the device demonstrated a technique for non-redundant selection of the storage-plane location. Figure 29 shows a reconstruction from a hologram formed in one of the tubes.

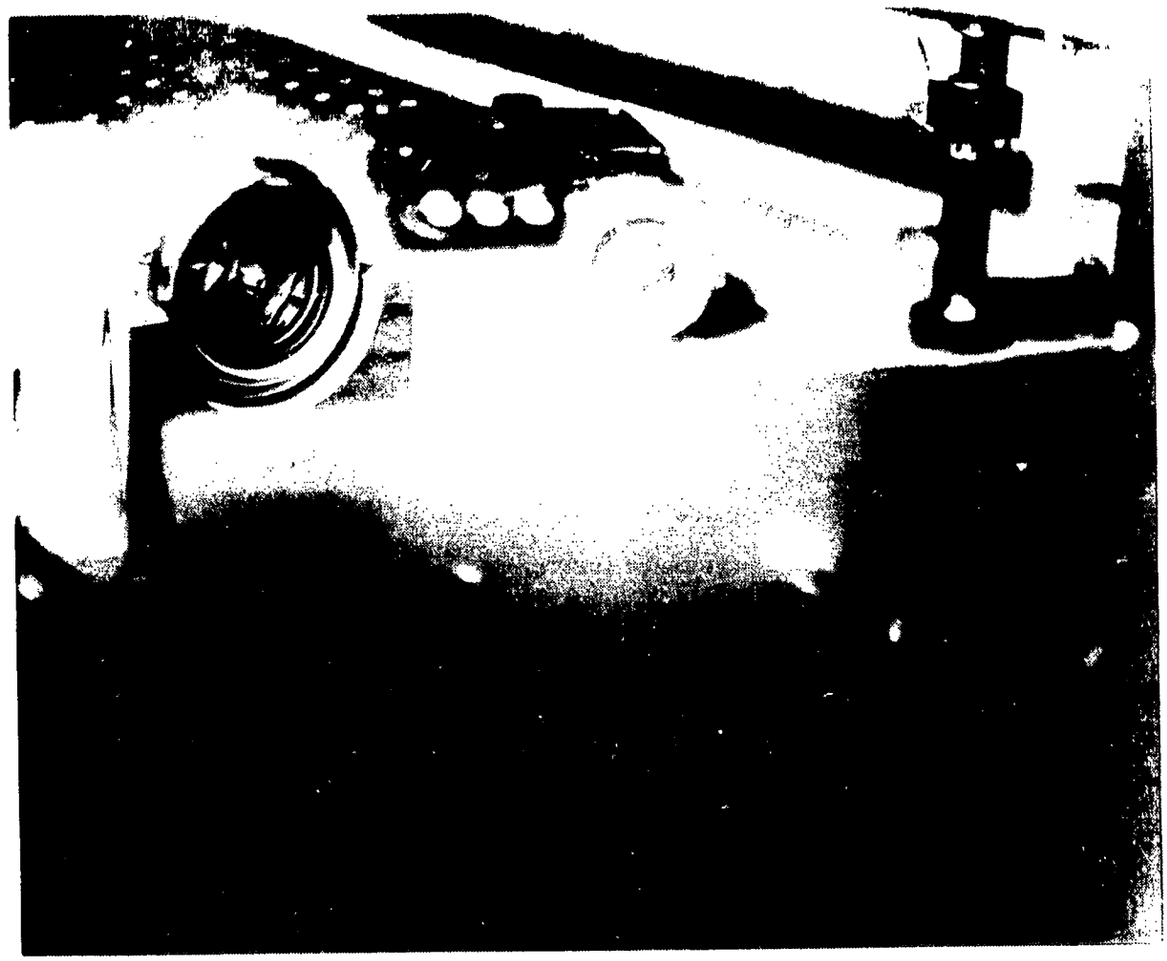

Figure 29. Electron image tube hologram reconstruction.

The stored holograms were quite weak, with an efficiency of less than 0.1%. The maximum efficiency, with one exception, was independent of: (1) the accelerating voltage, (2) the duration of the exposure, and (3) the amount of light from the auxiliary source which controlled the electron current.

The holograms that were formed were not erasable. No combination of accelerating voltage, beam current, or length of exposure led to even a small degree of erasure. New holograms could be formed on neighboring regions of the same target, but these too could not be erased.

Upon repeated operation the tube went gassy; that is, the pressure in the tube went from its initial value of less than 10^{-3} μm (10^{-6} torr) to a value close to atmospheric. The initial indication of this condition was the appearance of a slight blue glow in the tube (due to a plasma), which became more intense as operation was continued. The plasma finally became too dense to support an electric field across the tube. Holograms could be formed even in the presence of this plasma, as long as an electric field could be supported across the tube.

The operating life of the tube was 1-2 hours. The shelf life, that is, the lifetime of the tube when it was not operating, appeared to be unlimited. This indicated that material evolved from the thermoplastic under electron bombardment and subsequent heating caused the tube to become gassy. Later experiments with a demountable tube demonstrated that a considerable amount of material does evolve from the staybelite thermoplastic due to both heating and electron bombardment.

The low efficiency and the lack of successful erasure are not completely understood. Other experiments have demonstrated that the cesium used in activating the tube is adsorbed by the staybelite, and it is therefore reasonable to suppose that a change in the electrical resistivity caused by the cesium led to the low efficiencies observed, i.e., the film could not be sufficiently charged. Changes in the chemical and physical properties of the staybelite caused by the cesium and electron-beam bombardment can be assumed to be responsible for the lack of successful erasure. Since other materials, notably microcrystalline wax associated with complex styrene, have been found which withstand the ravages of cesium attack and electron beam bombardment, the exact nature of the chemical, physical and electrical changes was not pursued. However, the concept of hologram formation in an electron image tube was demonstrated, as was automatic selection of a page location with no additional selection mechanism.

D. Photoconductor Holographic-Recording Tube

1. Photoconductor tube description. — In order to take advantage of the high sensitivity and readout efficiency of the microcrystalline-wax storage media, and also the automatic page selection possible using image conversion principles, several tubes were designed and constructed containing holographic storage structures of the kind illustrated in Fig. 14. The storage structure consists of an InO-coated glass substrate, PVK photoconductor, microcrystalline wax, complex styrene coating, and aluminum surface electrodes. Although the styrene and surface electrodes are absent from Fig. 14, the entire structure, together with a recent photoconductor holographic-recording tube design is illustrated in Fig. 30.

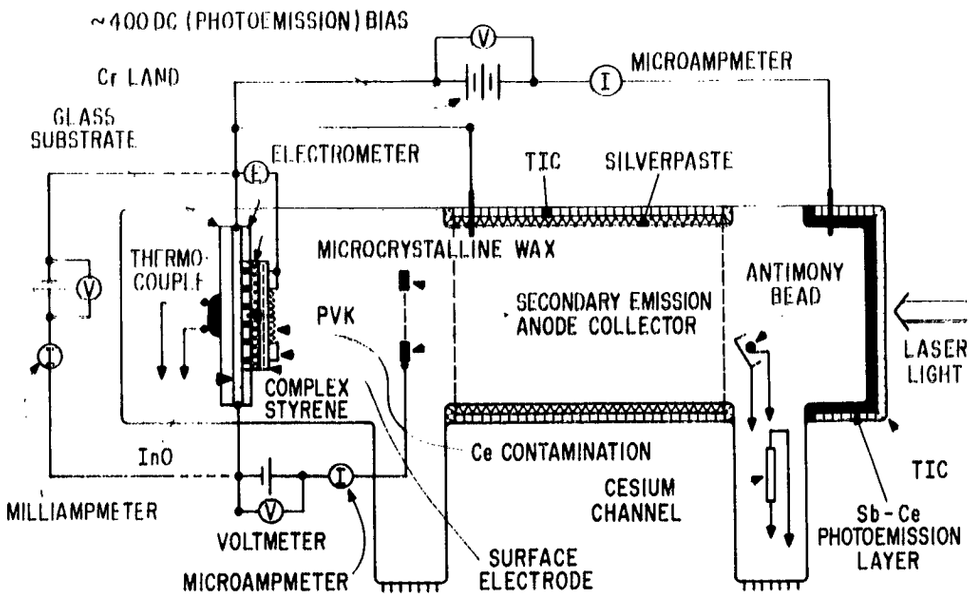

Figure 30. Holographic recording tube design.

As can be seen in the figure, the storage structure is at one end of the tube; a photoemissive cesium-antimony layer was deposited on the TIC-coated face of the tube opposite the storage device. A thermocouple was mounted behind and in contact with the glass substrate, and an anode collector was placed near the wax-complex styrene deformable surface. The anode collector was employed to measure secondary emission from the deformable surface during its bombardment by electrons photoemitted and electrostatically accelerated from the tube wall opposite the storage structure. An electrometer connected to the surface electrodes together with secondary-emission measurements were used to measure the potential of the deformable surface. Figure 31 is a photograph of one of the tubes in which another TIC coating was deposited along the length of the tube. This second TIC coating was deployed lengthwise in the tube and about its interior perimeter, and connected to the InO transparent electrode of the storage device. This latter TIC layer was used as a focusing electrode and enabled electrons originating from the photoemissive tube wall, due to the incident laser beam, to be focused at various locations on the deformable surface.

2. Cesium contamination. — The TIC layer along the tube wall was also coated with a layer of silver paste which served as a getter to prevent cesium released from a channel located at the photoemissive end of the tube from contaminating the storage device. However, in spite of these precautions cesium did reach the deformable surface and caused electrical leakage paths between it and the lands connected to the InO transparent electrode. These short circuits were sufficient to prevent the surface potential from climbing above ~40 V under conditions of maximum photoemission current (~250 μA). Attempts were made to use the surface electrodes to sustain surface

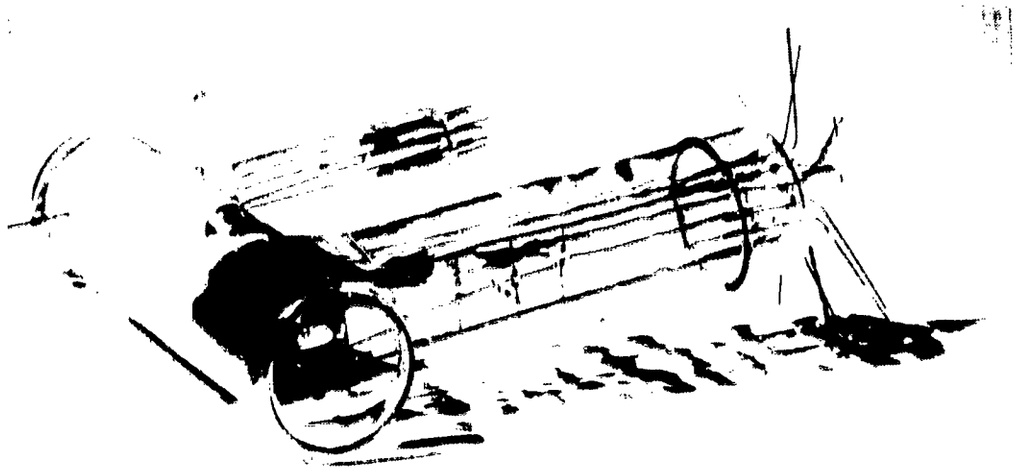

Figure 31. Photograph of holographic recording tube.

potentials of the order of several hundred volts, i.e., levels adequate for holographic recording. An external battery was connected to the aluminum electrodes, but excessive ohmic heating caused discontinuation of the experiment.

3. Page selection. — It had been hoped that the holographic page could be selected through heat supplied by photoemitted electrons via the light selection mechanism itself, thereby eliminating the need for matrix-type ohmic heaters, and the additional problem areas that they engender. In addition, the automatic thermal page selection would have provided a minimum heat loss because of the concentration and dissipation of heat exactly at the desired page location. These advantages did not materialize, however, because of the electrical leakage paths incurred through contamination of the storage structure by cesium.

E. Photoemission Holographic Recording Tube

1. Page selection. — Several tubes were designed and constructed in work oriented toward the recording of holograms using photoemission from the deformable surface. In this approach, two photocathodes are employed in the tube. One photocathode is made in the usual way by depositing a layer of antimony and cesium on top of the TIC-coated tube wall opposite the storage structure. The second photocathode involves a more complicated procedure, which results in a very-high-impedance photoemissive coating along the surface of the deformable medium. The photocathode at the tube wall opposite the storage device provides electrons in response to the incident laser beam, which are electrostatically accelerated and focused at a location on the deformable surface dictated by the particular address present at the laser deflection system. The heat dissipated at this location due to the bombardment of these electrons thus permits automatic

page selection. The photoemissive coating on the storage device provides the means for establishing a charge pattern along the deformable surface in a one-to-one relation to the holographic-intensity pattern caused by the interference of the object and reference beams. (The photoconductor layer of previous systems was an alternative way of establishing that charge pattern.)

2. Photoemissive deformable surface. — The problem of creating a photoemissive coating along the microcrystalline-wax surface turned out to be formidable because of the poor vapor pressure of the wax, and the propensity of detrimental chemical reaction between it and the cesium. It was discovered, however, that the molecular saturation present in the complex-styrene films (discussed earlier under material fatigue) enabled these films to remain chemically stable when exposed to cesium in high vacuum with no discernible reaction between the styrene and the cesium. Therefore, procedures were developed for polymerizing and crosslinking the styrene directly onto the surface of the microcrystalline wax. Tubes were constructed which contained the composite wax-complex styrene structures, and techniques were developed whereby a photoemissive coating was deposited on the complex-styrene films. These techniques permitted optimization of the photoelectric sensitivity of such coatings. Figure 32 is a photograph of one such tube in which the photoelectric sensitivity was measured to be 23 mA/W at 400-nm wavelength, and 6 mA/W minimum throughout the wavelength interval from 350 nm to 550 nm. Figure 33 is a plot of the measured sensitivity. The tube was sealed at a pressure of 10^{-5} μm (10^{-8} torr),

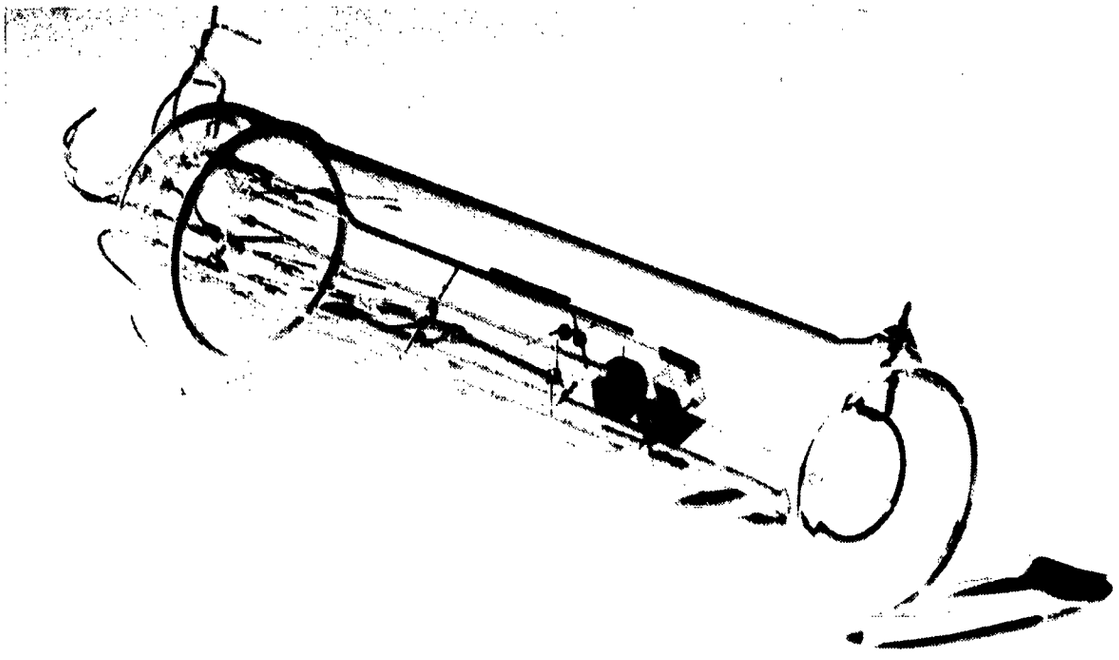

Figure 32. Photograph of photoemissive tube.

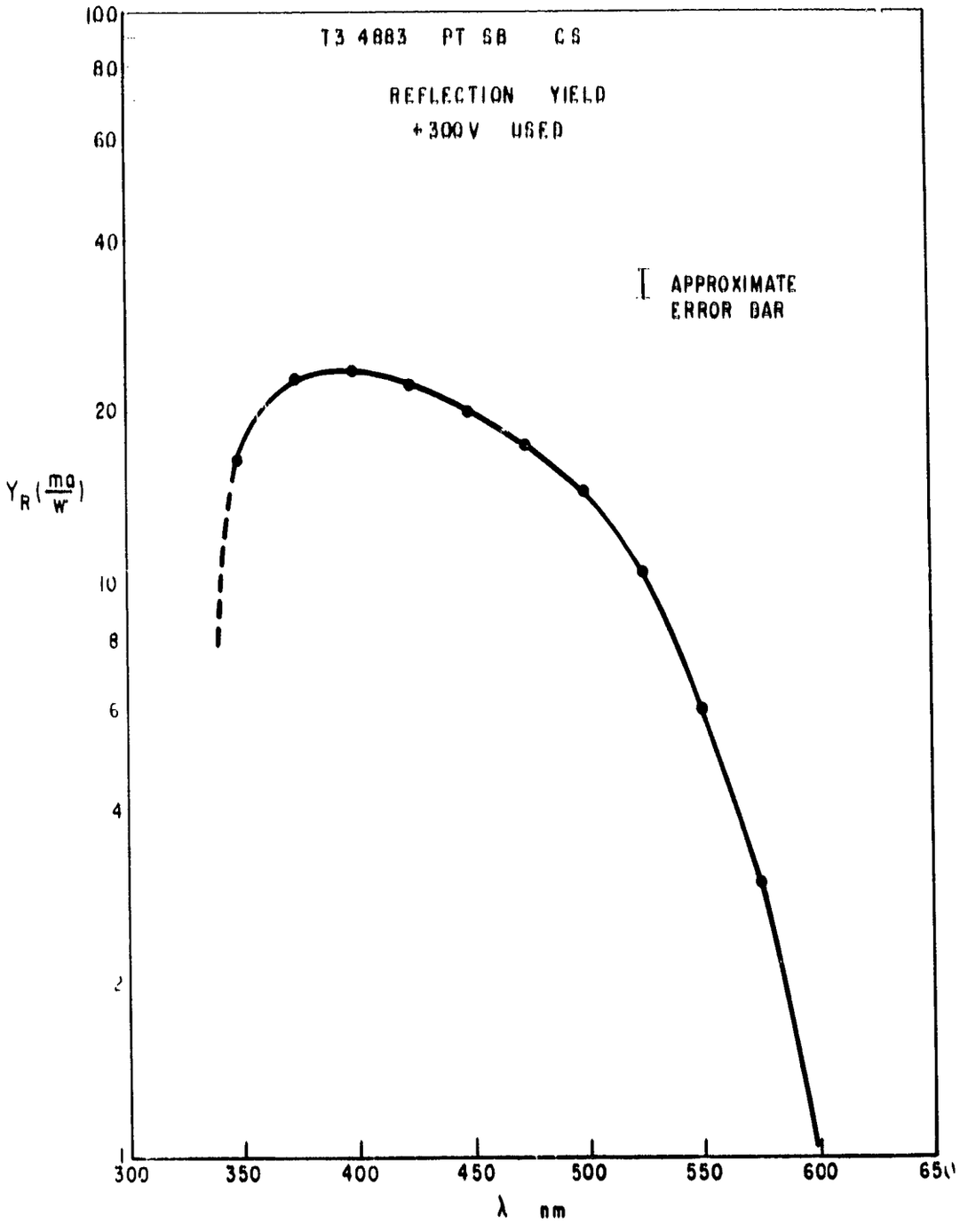

Figure 33. Plot of measured photoelectric sensitivity vs. wavelength.

and measurements of the photoelectric sensitivity taken after a 9-day period showed the same values as those exhibited by the tube at the time it was sealed. These measurements show that the pressure within the tube did not appreciably increase after a 9-day period, and indicate that the cesium does not react with the complex-styrene film in such an environment. Similar results were obtained in later experiments, thereby confirming the capacity of the highly polymerized and crosslinked styrene to protect the wax in high vacuum from adverse reaction with cesium at temperatures at which the wax deforms. This work also established the capacity of the wax complex styrene-composite structure to withstand bake-out temperatures of 100 C over a 24-hour period.

3. Photoemission tube description. Tubes were designed and constructed with the structure shown in Figs. 30 and 31. The target structure was as shown in Fig. 34, and consisted of an InO-coated glass substrate, microcrystalline-wax film, complex-styrene coating, aluminum surface electrodes, and a layer of antimony and cesium deposited using procedures which maximized the photoemission from the deformable surface. A surface resistivity of 5 megohms per square was measured between the two surface electrodes, and the photoelectric sensitivity was observed to be about 1 μA per 10 mW of incident laser power at a wavelength of about 442 nm.

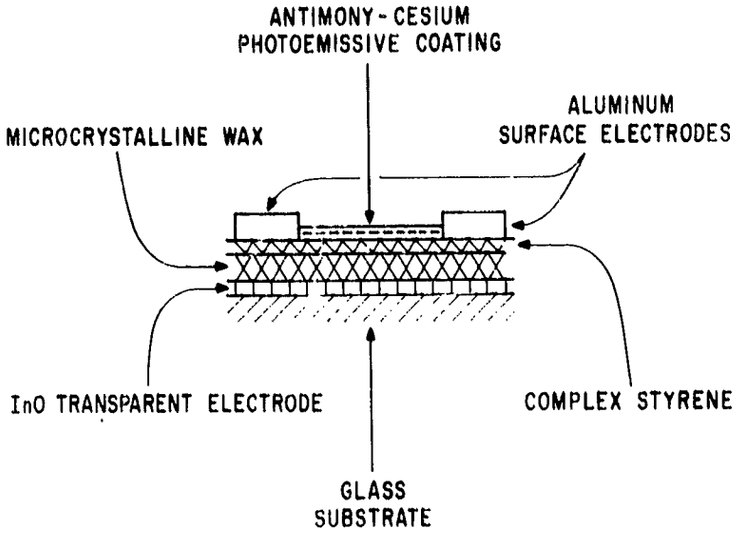

Figure 34. Device structure for use in holographic recording tube.

4. Surface resistivity. – All attempts at recording holograms by means of the photoemissive mechanism from the deformable wax-styrene composite surface failed. One reason for the failure was due to the comparatively low surface resistance (~megohms/square). At typical levels of photoemissive current, it was simply not possible to maintain adequate surface potential using only photoemission.

5. Photoemissive holography versus deformation stability. — As discussed in Appendix A, stable deformations require that the change in surface energy necessary for a portion of the film surface to reach the transparent electrode within a half-period of the pattern exceed the electrostatic energy originally stored in the same half-period. However, the detailed discussion in Appendix C of the recording of holograms using a photoemission mechanism shows that when this stability criterion is satisfied, the charge is differentially distributed along the deformable surface due to photoemission processes, and homogeneously redistributes prior to the onset of surface depressions. In Appendix C, it is shown that the time t necessary to deform the surface an amount Δs due to a differential charge via a photoemission current of magnitude i_0 is

$$t = \frac{RC}{2(r-1)} \ln \frac{8 E_c \Delta s}{i_0 R f(r)} \tag{13a}$$

where R and C are the resistance and capacitance of the holographically defined regions, E_c the dielectric breakdown field of the microcrystalline-wax complex-styrene composite coating, and r twice the ratio of the electrostatic stress (ϵE_c^2) to the elastic stress (ξ), where

$$f(r) = \frac{r}{r-1} \left[1 + \frac{1}{(r-1)(r-2)} \right] \tag{13b}$$

It is clear from Eqs. (13a,b), that holographic depressions occur only if the ratio of electrostatic-to-elastic stress exceeds unity. However, as shown in Appendix A, the onset of such deformations is not energetically stable, but instead produces a condition of frost, the presence of which was observed during evaluation of the photoemission holographic-recording tube.

F. Laser Addressed Holographic Storage Chamber

1. Heat transfer. — The work reported above on the holographic recording tubes served to emphasize a fundamental and detrimental characteristic common to vacuum type environments viz., such tubes are not suitable for thermoplastic holographic storage where heat must be transferred to and from the storage device. Investigations performed on the space-charge, neutralized, demountable storage chamber discussed earlier (e.g., see Fig. 16) yielded similar thermal decay behavior. Unlike the high vacuum $\sim 10^{-5}$ μm ($\sim 10^{-8}$ torr) tubes discussed above, the pressure within the demountable, glow-discharge chamber was of the order of 5×10^5 μm (500 torr). Yet, despite the appreciably higher pressure, heat transfer from the substrate of the storage device remained poor ($\sim$ seconds).

2. Demountable storage chamber. — The long thermal-decay time was an unfortunate result because of the many advantages such a chamber had to offer. The dc bias of the molecules of the space-charge neutralized glow provided a uniform potential across the surface of the holographic-storage media. The 5×10^5 μm (500 torr) inert atmosphere of the chamber also provided an environment free of ambient fluctuations, thereby permitting practical maintenance of stable-temperature bias to the holographic-storage device. The chamber was to be used in a unique system, in which thermal bias in conjunction with heat produced directly from absorption of the laser beam by the storage device would automatically select holographic pages at desired locations. Several demountable chambers were designed and constructed which provided for addressing over a 2-cm by 2-cm area. A photograph of one such chamber, including keeper electrodes (used as a constant source of ions via a small dc potential) is shown in Fig. 35. In an effort to assist the transfer of heat from the substrate through increased pressure, measurements were taken of the dc electrical resistance of the chamber versus pressure for an argon inert atmosphere. The data is plotted in Fig. 36, where an optimum pressure is seen to occur at $\sim 5 \times 10^5$ μm ($\sim$500 torr).

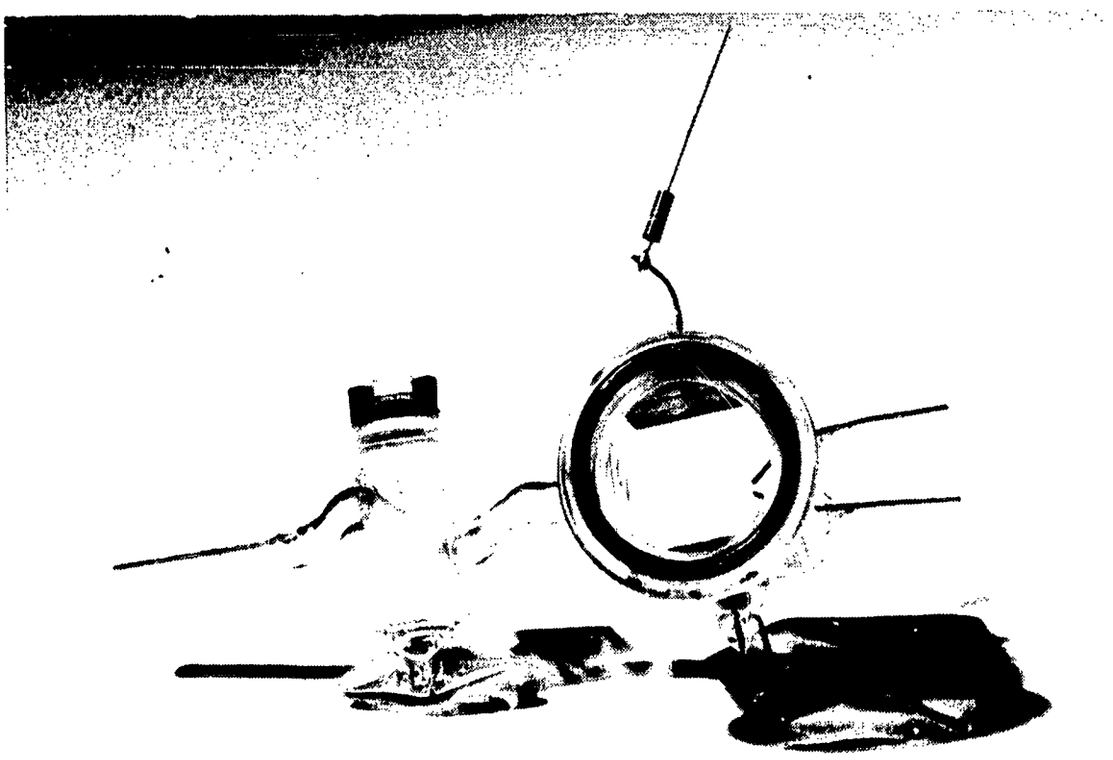

Figure 35. Photograph of 2-cm by 2-cm demountable glow chamber.

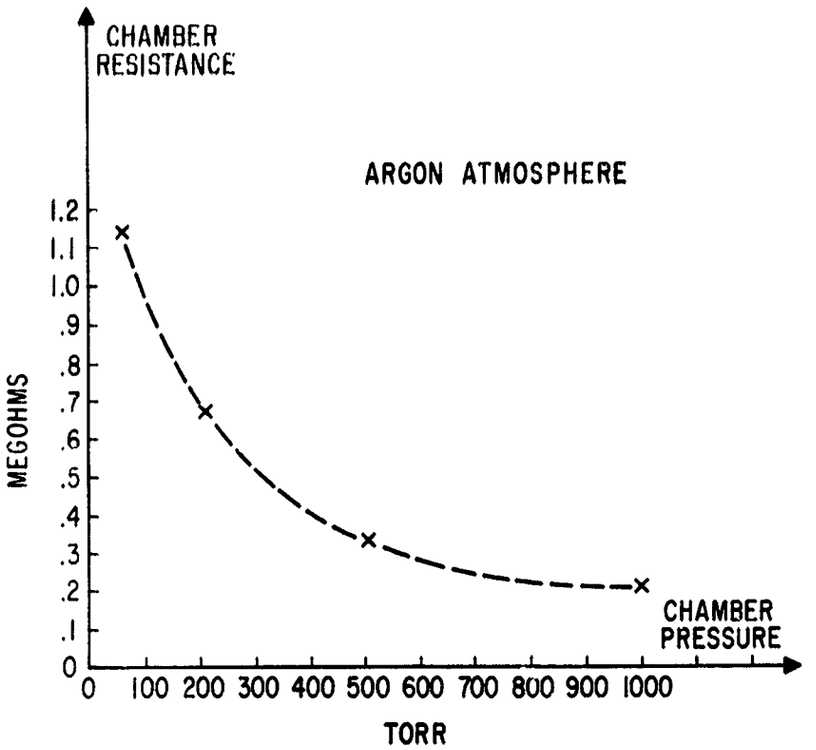

Figure 36. Plot of glow chamber resistance vs. pressure.

3. Corona grid structure. — Because of the cooling effect implicit in a corona discharge, and the promise of more rapid thermal decay, work was initiated on a demountable, multiple-grid structure operating under ambient pressure and corona-type discharge. Two-dimensional grids were constructed over areas in excess of 4 cm^2 using various wires ranging from 45 μm to 125 μm in diameter. Three kinds of grid structures were designed, constructed, evaluated and found to be unsatisfactory due to spacially-nonuniform charging characteristics, and day-to-day changes in discharg properties. Although improvement was obtained through the use of grids of finer mesh, the constraint of random access over a 4 cm^2 area limited the number, diameter, and surface of the wires which could be employed.

4. Corona chamber. — The basic problem was that of providing uniform charge to the deformable surface over an area of at least 2 cm by 2 cm at ambient pressure, thereby allowing sufficient heat transfer from the storage device. An approach which proved to be successful in providing uniform charge, and through which holograms were satisfactorily recorded over a 2-cm by 2-cm area involved the use of a unique corona-discharge device, in which high voltage was supplied to a single-discharge needle via a two-dimensional electrostatic shield positioned orthogonal to the needle, and parallel to the deformable surface. The structure is illustrated in Fig. 37. The discharge needle was symmetrically separated from the deformable surface over a

distance adequate to provide a charge shadow in excess of 2 cm by 2 cm. A separation somewhat larger than 2.5 cm proved adequate, and this necessitated a corona voltage of about 15 kV.

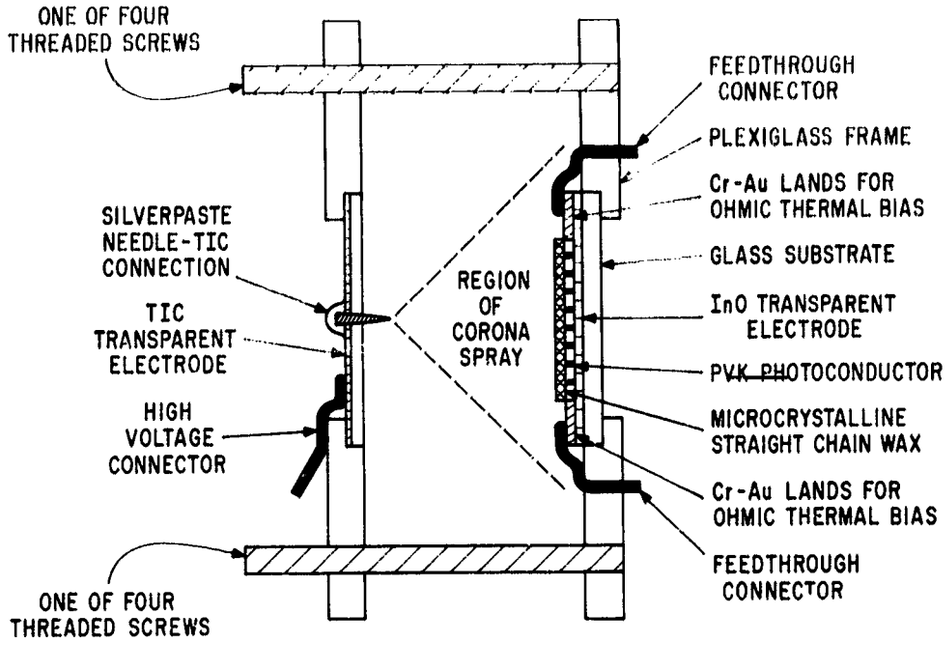

Figure 37. Corona discharge structure design.

5. Chamber description. -- The corona structure consists of a 1.2-cm-long discharge needle positioned through a 375 μm hole ultrasonically drilled in a glass substrate, which is TIC coated on one side. The high-voltage connection to the needle is made via the TIC coating through a plexiglass frame in which the substrate is mounted. Care was taken to ensure that the TIC-coated discharge substrate was parallel to the deformable surface with the separation between the needle and the deformable surface controlled by means of four threaded screws, which connected the corona-discharge substrate and the storage device. The region of corona spray was insulated from effects of external air currents by means of a plexiglass shield placed about the corona-discharge structure. The shield contained demountable spacers, and a frame through which holes were drilled, ensuring equilization of ambient pressure to that inside the chamber. The shield also served to stabilize the temperature of the storage device during constant-corona exposure due to thermal bias via a dc current through the transparent electrode. A photograph of the corona-discharge chamber is shown in Fig. 38.

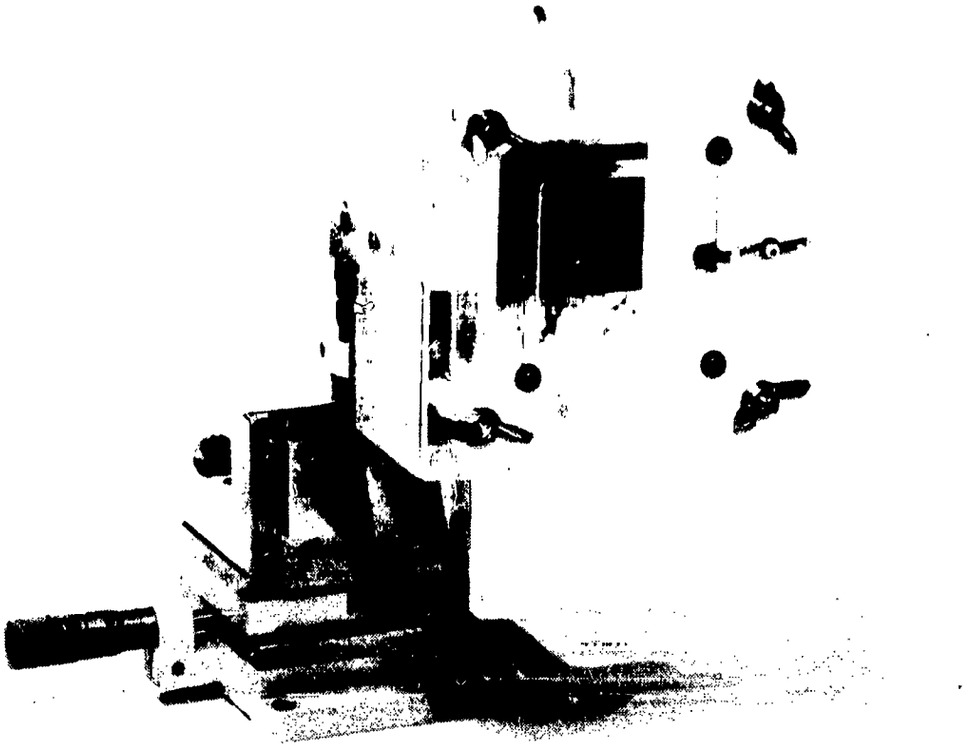

Figure 38. Photograph of corona discharge chamber.

6. Laser-addressed storage device. — As indicated earlier in the sections on the photoconductor and photoemissive holographic-recording tubes, work on such tubes was motivated by the promise that matrix-type ohmic heaters could be eliminated, and that automatic holographic page selection would occur via photoemitted electrons in response to the laser beam. In addition, the tubes promised a means of uniformly supplying charge to the deformable storage media. Although these tubes did not behave in the desired manner for the reasons discussed earlier, the work did lead to the successful development of a configuration in which charge is provided sufficiently uniform over practical areas, and holographic pages are completely selected by means of the laser-deflection system at reasonable power levels. The corona-discharge chamber, which provides a continuous and uniform charge spray is discussed above and illustrated in Fig. 37. The corona structure was used in conjunction with a microcrystalline-wax photoconductor storage device to successfully store and erase holograms over the large area. Ohmic heating was used to thermally bias the wax to below its melting temperature, and an argon laser was employed to provide the additional power (~80 mW), which at selected locations, melted the wax in conjunction with the thermal bias

common to the large area. The successful recording and erasure of holograms by the laser beam was possible only because of the sharp (~2°C) transition temperature of the microcrystalline-wax storage media. A continuous corona discharge was used throughout the read/write cycles, and a helium-neon (~1.0 mW) laser provided the two-beam interference pattern. The experimental arrangement is shown in Fig. 39; the arrangement allowed convenient argon-laser (heat) switching by simply opening and closing a shutter as shown in Fig. 39. Page selection was done by manually moving the storage device with respect to the laser beams. System deployment of the laser addressed wax phase transition would incorporate a single laser in conjunction with an electronic light modulator as shown in Fig. 40.

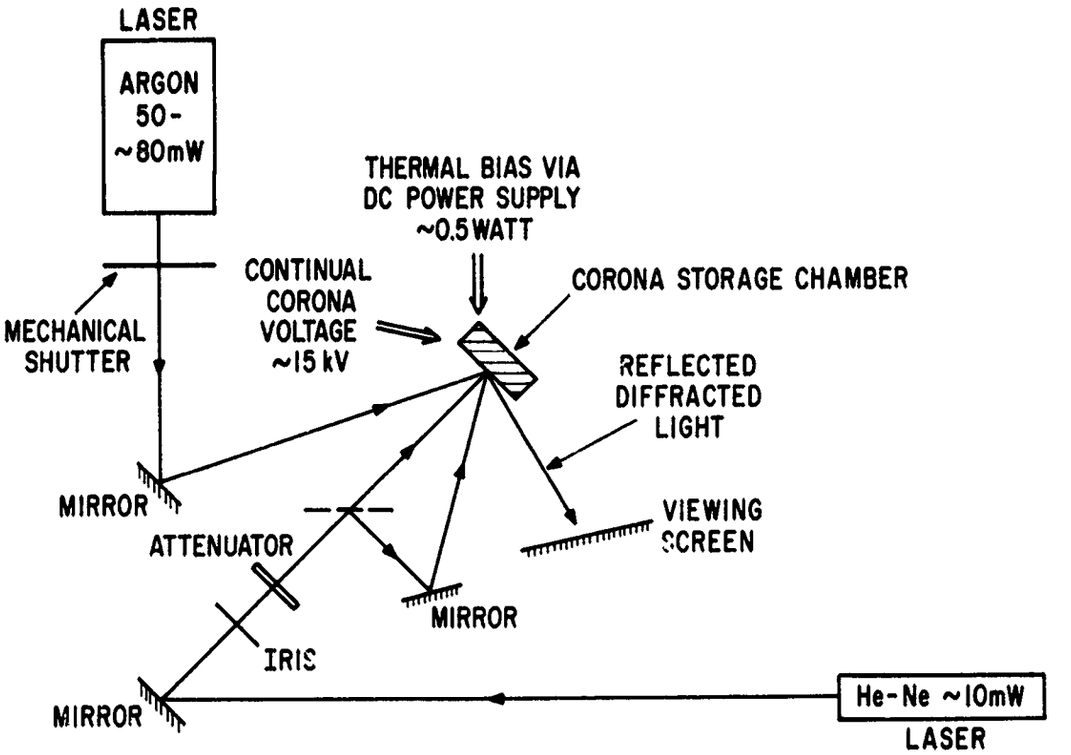

Figure 39. Experimental arrangement of laser addressed memory.

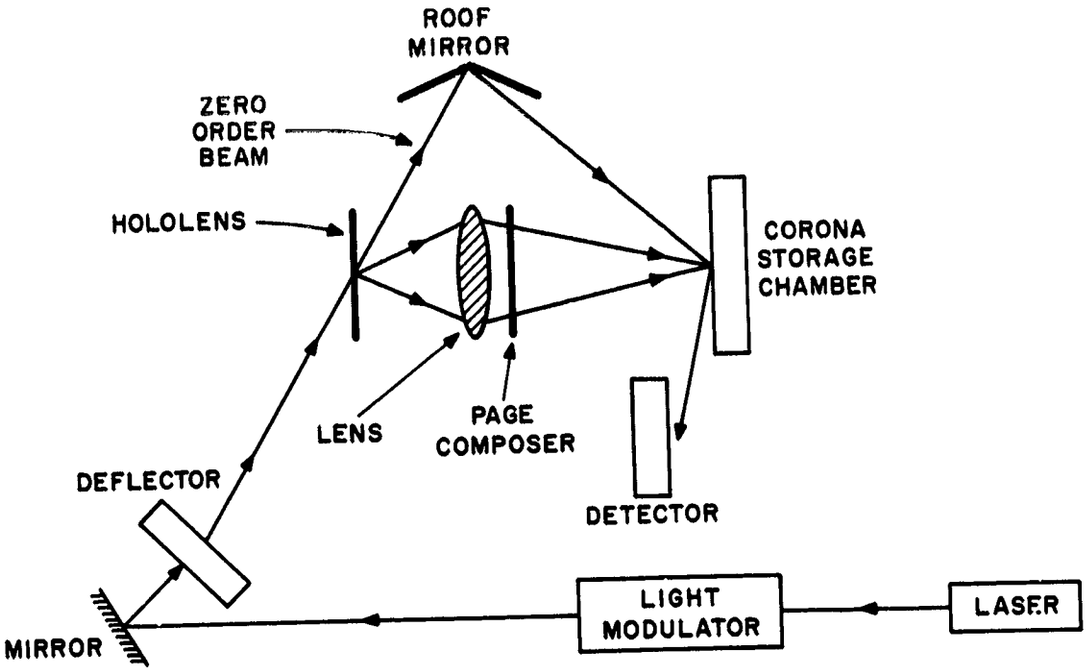

Figure 40. System configuration of laser addressed memory.

VI. CONCLUSIONS

The objective of this research was to investigate the use of thin deformable films as the storage medium in a high-speed, random-access, read/write holographic memory.

The main conclusion to be drawn from the work is that deformable films which use heat as a a part of the recording process are not satisfactory for this application, because of fundamental thermal considerations. On the basis of both theoretical analysis and experimental evidence, it was found that the heating time and cooling time of a small area in a film subjected to local heating are in the ratio of approximately 1:1000. If the memory is to be truly random access, a time equal to 1000 heating times must elapse between successive write and erase operations. Heating times of the order of 100 μsec to 1 msec are possible, but even these result in cycle times of 100 msec and 1 sec, respectively, which are too long for a high speed memory. Thus, in order to use heat deformable films, one must give up either high speed or random access. We emphasize the the restrictive nature of our conclusions because heat deformable media are well suited to serially accessed systems, particularly those in which the medium moves, because this permits very simple charging and heating stations.

The fatigue problem, which plagued thermoplastics for many years, does not appear to be as formidible as it once seemed. One material that was developed during this contract has shown no fatigue after more than 7000 cycles.

The two other major problems, i.e., charging and selective heating, are both tied to random accessibility. In a serial accessed system neither presents any fundamental difficulties.

APPENDIX A

Surface Deformation in Microcrystalline Wax

Assume the wax to be distorted by a sinusoidal charge distribution deposited through the interference of two laser beams on a photoconductor as

$$\sigma(x) = \sigma_o + \sigma_1 \cos kx \tag{A1}$$

where $k = 2\pi/d$.

Application of heat from underneath by ohmic heating of the transparent electrode permits the electrostatic forces to displace the liquified wax from regions of high-charge concentration to those of low-charge concentration. During this time, the charge is assumed essentially immobile on the distorted, but yet solid surface. The distortion will, in general, be maintained even when the film is completely liquified, and the surface charge can be regarded as mobile on the surface as a result of the higher image forces in the high-charge regions as compared to that in the low-charge regions. If the increase in surface energy necessary for a portion of the film surface to reach the transparent electrode within a half-period of the pattern, exceeds the electrostatic energy originally stored in the same half-period, then the wax film will assume a stable-distorted form with the period of the original-charge distribution. If this condition does not occur, then spontaneous frost formation will be observed as the wax is liquified. Assuming an equilibrium distortion, then the surface and electrostatic energies will acquire a minimum value over one-half of the period d.

An approximate stability criterion is derived as follows: assume the surface contour y(x) is sinusoidal, i.e.,

$$s(x) = s_o - s_1 \cos kx \tag{A2}$$

where s_o is the original wax thickness, then the increase in surface energy attributable to the distortion is

$$W_s = T \int_0^{d/2} \left\{ \left[1 + \left(\frac{ds}{dx} \right)^2 \right]^{1/2} - 1 \right\} dx$$

$$= \frac{d}{\pi} \int_0^{\pi/2} \left[\left(1 + a^2 \sin^2 \theta \right)^{1/2} - 1 \right] d\theta \tag{A3}$$

$$= \frac{1}{2} Td\left(\frac{a}{2}\right)^2 \left(1 - \frac{3}{8}a^2 + \frac{5}{32}a^4 - \frac{175}{2048}a^6 + \right) \tag{A4}$$

where $a = ks_1$ and T is the per-unit-area surface energy. The stability criterion is that W_s for $s = s_1$ be greater than the electrostatic energy of the half period for $k = 0$

$$W_s > \frac{d}{4s_o} \epsilon V^2 \tag{A5}$$

where V is the potential impressed on the wax surface.

Initially, after the charge deposition given by Eq. (A1) on the flat surface, the potential distribution is

$$\phi_1(x,y) = A_o y + \sum_{n=1}^{\infty} A_n \sinh(kny) \cos(knx) \tag{A6a}$$

for $y < s$

and

$$\phi_2(x,y) = B_o + \sum_{n=1}^{\infty} B_n \exp(-kny) \cos(knx) \tag{A6b}$$

for $y > s$

Using the following boundary conditions

$$\sigma(x,s) = \epsilon_1 \left(\frac{\partial \phi_1}{\partial y}\right)_s - \epsilon_o \left(\frac{\partial \phi_2}{\partial y}\right)_s \tag{A7a}$$

$$\phi_1(s) = \phi_2(2) \tag{A7b}$$

the potentials solve as

$$\phi_1(x,y) = \frac{\sigma_o}{\epsilon_1} \left[y + \frac{\sigma_1}{k\sigma_o} \cos kx \frac{\sinh ky}{\cosh ks + \frac{1}{k} \sinh ks} \right] \tag{A8a}$$

$$\phi_2(x,y) = \frac{\sigma_o}{\epsilon_1} \left[s + \frac{\sigma_1}{k\sigma_o} \cos kx \frac{\exp[-k(y-s)]}{\frac{1}{k} + \coth ks} \right] \tag{A8b}$$

When the film has completely liquified, the charge can distribute itself along the surface which becomes an equipotential of magnitude V. The potential distribution within the film at $y < s(x)$ is given by Eq. (A6a) with new values for the coefficients A_n, whereas for $y > s(x)$, $\phi_2(x,y) = 0$. The coefficients A_n are now determined by the single boundary condition

$$A_o\, s(x) + \sum_{n=1}^{\infty} A_n \sinh(kn\, s(x)) \cos(knx) = V \tag{A9}$$

for $\qquad 0 \leq x \leq d/2$

under the constraint

$$\epsilon_1 \int_0^{d/2} \frac{\partial \phi_1}{\partial y}_{s} \left[1 + \left(\frac{ds}{dx}\right)^2\right] dx = \int_0^{d/2} \sigma(x)\, dx \tag{A10}$$

Noting that

$$\sinh\Big(kn\, s(x)\Big) = \sinh(kn s_o)\left[I_o(kn s_1) + 2\sum_{m=1}^{\infty} I_{2m}(kn s_1)\cos(2mkx)\right] - \cosh(kn s_o)\left\{2\sum_{m=0}^{\infty} I_{2m+1}(kn s_1)\cos\left[k(2m+1)x\right]\right\} \tag{A11}$$

$$\cosh(kn\, s(x)) = \cosh(kn s_o)\left\{I_o(kn s_1) + 2\sum_{m=1}^{\infty} I_{2m}(kn s_1)\cos(2mkx)\right\} - \sinh(kn s_o)\left\{2\sum_{m=0}^{\infty} I_{2m+1}(kn s_1)\cos\left[k(2m+1)x\right]\right\} \tag{A12}$$

substitution of Eq. (A11) into (A9) yields the set of simultaneous equations for the coefficients A_n as

$$A_o s_o + \sum_{m=0}^{\infty} A_{2m} I_{2m}(2m)\sinh(2m) - \sum_{m=0}^{\infty} A_{2m+1} I_{2m+1}(2m+1)\cosh(2m+1) = V \tag{A13a}$$

$$- A_o s_1 + \sum_{m=0}^{\infty} A_{2m+1}\left[I_{2m}(2m+1) + I_{2m+2}(2m+1)\right]\sinh(2m+1)$$

$$- \sum_{m=0}^{\infty} A_{2m+2}\left[I_{2m+1}(2m+2) + I_{2m+3}(2m+2)\right]\cosh(2m+2) = 0 \qquad \text{(A13b)}$$

$$\sum_{m=0}^{\infty} A_{2m+2}\left[I_{2m+4}(2m+2) + I_{2m}(2m+2)\right]\sinh(2m+2)$$

$$\text{(A13c)}$$

$$- \sum_{m=0}^{\infty} A_{2m+3}\left[I_{2m+1}(2m+3) + I_{2m+5}(2m+3)\cosh(2m+3) - A_1\, I_1(1) + I_3(1)\right]\cosh(1) = 0$$

for even $N > 2$

$$\sum_{m=0}^{\infty} A_{2m+N}\left[I_{2m}(2m+N) + I_{2m+2N}(2m+N)\right]\sinh(2m+N)$$

$$- \sum_{m=0}^{\infty} A_{2m+1+N}\left[I_{2m+1}(2m+1+N) + I_{2m+1+2N}(2m+1+N)\right]\cosh(2m+1+N)$$

$$+ \sum_{m=1}^{(N-2)/2} A_{2m}\left[I_{N-2m}(2m) + I_{N+2m}(2m)\right]\sinh(2m)$$

$$\text{(A13d)}$$

$$- \sum_{m=0}^{(N-2)/2} A_{2m+1}\left[I_{N-1-2m}(2m+1) + I_{N+1+2m}(2m+1)\right]\cdot \cosh(2m+1) = 0$$

For odd $N > 2$

$$\sum_{m=0}^{\infty} A_{2m+N}\, I_{2m}(2m+N) + I_{2m+2N}(2m+N)\, \sinh(2m+N)$$

$$- \sum_{m=0}^{\infty} A_{2m+1+N}\left[I_{2m+1}(2m+1+N) + I_{2m+1+2N}(2m+1+N)\right]\cosh(2m+1+N)$$

$$- \sum_{m=0}^{(N-3)/2} A_{2m+1}\left[I_{N-1-2m}(2m+1) + I_{N+1+2m}(2m+1)\right]\sinh(2m+1) \qquad (A13c)$$

$$- \sum_{m=0}^{(N-3)/2} A_{2m+2}\left[I_{N-2-2m}(2m+2) + I_{N+2+2m}(2m+2)\right]\cosh(2m+3) \quad 0$$

The argument of the Bessel function I_n (of imaginary argument) in Eqs. (A13a-c) must be multiplied by ks_1; similarly the argument of the hyperbolic functions sinh, cosh, must be multiplied by ks_o.

Substitution of Eqs. (A2) and (A6a) into (A10) gives

$$\int_0^{d/2} \left\{A_o + \sum_{n=1}^{\infty} kn\, A_n \cosh\left[kns(x)\right]\cos(knx)\right\}\left\{1 + \frac{1}{2}(ks_i)^2\left[1 - \cos\left(\frac{kx}{2}\right)\right]\right\} dx = \frac{\sigma_o d}{2\epsilon_1} \qquad (A14)$$

or

$$\frac{A_o d}{2}\left[1 + \frac{1}{2}(ks_1)^2\right] + \int_0^{d/2}\left\{\sum_{n=1}^{\infty} kn A_n \cosh\left[kns(x)\right]\right\}$$

$$\cdot\left\{\left[1+\frac{1}{2}(ks_1)^2\right]\cos(knx) - \frac{1}{4}(ks_1)^2\left[\cos(k[n+2]x) + \cos(k[n-2]x)\right]\right\} dx = \frac{\sigma_o d}{2\epsilon_1} \qquad (A15)$$

Substitution of Eq. (B-12) into B-15 gives

$$\left\{\left[1+\frac{1}{2}(ks_1)^2\right]\left\{(A_o/k)+\sum_{m=1}^{\infty} 2m\, A_{2m}\, I_{2m}(2m)\cosh(2m)\right.\right.$$

$$\left.-\sum_{m=0}^{\infty}(2m+1)\,A_{2m+1}\,I_{2m+1}(2m+1)\sinh(2m+1)\right\}$$

$$-\frac{1}{4}(ks_1)^2\left\{\sum_{m=0}^{\infty}(2m+2)\,A_{2m+2}\cosh(2m+2)\left[I_{2m}(2m+2)+I_{2m+4}(3m+2)\right]\right\}$$

$$-\sum_{m=0}^{\infty}(2m+3)\,A_{2m+3}\sinh(2m+3)\left[I_{2m+1}(2m+3)+I_{2m+5}(2m+3)\right] \qquad (A16)$$

$$\left.-A_1\left[I_1(1)+I_3(1)\right]\sinh(1)\right\}=\frac{\sigma_o}{k\epsilon_1}$$

Equation (A16) relates the potential V along the surface of the wax to the charge density (σ_o). Assuming small amplitudes of deformation such that

$$I_o(n) \approx 1+\frac{1}{4}(nks_1)^2 \qquad (A17a)$$

$$I_1(n) \approx \frac{1}{2}\,nks_1 \qquad (A17b)$$

$$I_2(n) \approx \frac{1}{8}(nks_1)^2 \qquad (A17c)$$

and limiting the terms to second order in s_1, Eqs. (A13) and (A16) yield

$$A_o \approx (V/s_o)\left[1+\frac{s_1^2}{s_o d}\coth(ks_o)\right] \qquad (A18a)$$

$$A_1 \approx (s_1 V/s_o)\cosh(ks_o) \qquad (A18b)$$

$$A_2 \approx (ks_1^2 V/4s_o)\,\mathrm{csch}^2(ks_o) \qquad (A18c)$$

The electrostatic energy is

$$W_e = \frac{1}{2}\epsilon_1 \int_0^{d/2} dx \int_0^{s(x)} \left[\left(\frac{\partial \phi_1}{\partial x}\right)^2 + \left(\frac{\partial \phi_1}{\partial y}\right)^2\right] dy$$

$$= \frac{1}{4}\epsilon_1 s_o d \left[\Lambda_o^2 - \frac{k s_1}{s_o} \Lambda_o \Lambda_1 \coth k s_o + \left(\frac{\pi \Lambda_1}{d}\right)^2 \left(\frac{\sinh 2 k s_o}{2 k s_o} - 1\right)\right] \qquad \text{(A19)}$$

$$= \frac{1}{4}\epsilon_1 (d/s_o) V^2 \left[1 + \frac{1}{4}(k s_1)^2 \left(\frac{\coth k s_o}{k s_o} - \operatorname{csch}^2 k s_o\right)\right]$$

Noting that Eq. (A16) gives the surface potential as

$$V = \frac{s_o \sigma_o}{\epsilon_1}\left(1 - \frac{k s_1^2}{2 s_o} \coth k s_o\right) \qquad \text{(A20)}$$

the electrostatic energy is

$$W_e = \frac{s_o d}{4\epsilon_1} \sigma_o^2 \left[1 - \frac{3}{4}\frac{k s_1^2}{s_o} \coth k s_o - \frac{1}{4}(k s_1)^2 \operatorname{csch}^2 k s_o\right] \qquad \text{(A21)}$$

There are two limits to consider viz.

$$W_e \approx \frac{s_o d}{4\epsilon_1} \sigma_o^2 \left[1 - \left(\frac{s_1}{s_o}\right)^2\right] \qquad \text{(A22a)}$$

for $k s_o << 1$

and

$$W_e \approx \frac{s_o d}{4\epsilon_1} \sigma_o^2 \left(1 - \frac{3}{4}\frac{k s_1^2}{s_o}\right) \qquad \text{(A22b)}$$

for $k s_o >> 1$

Equations (A22a,b) show that for thicknesses of wax small compared to the period of the disturbance, the energy change for a given surface charge density (σ_o) is proportional to the wax thickness (s_o); for

wax thicknesses large compared to d, the energy change is proportional to s_o^2/d. The onset of spontaneous deformation, i.e., frost, occurs with periods longer than d [Eq.(A4)] when

$$|\delta W_e| = W_s = \frac{\pi k s_1^2 T}{4} \tag{A23a}$$

i.e., for

$$d > \frac{\pi}{\epsilon_o} (2\epsilon_1 s_o T)^{1/2} \tag{A23b}$$

with $k s_o << 1$

and

$$d > \frac{4\pi\epsilon_1}{3\sigma_o^2} T \tag{A23c}$$

with $k s_o >> 1$

For large values of s_o, the frost spectrum is independent of s_o, whereas for small values, the limiting frost wavelength decreases with the square root of s_o. Note that the stability criterion of Eq. (A23b) corresponds exactly to that of Eq. (A5).

The assumption of free-mobile charge on the wax surface may not, in general, be completely valid. However, in this instance many ad hoc assumptions then become necessary. Taking $\sigma(x)$ to be the actual charge density, the effective charge density $\phi(x)$ is then given as

$$\phi(x) = \sigma(x) + (\epsilon_1 - \epsilon_o) \left\{ \left(\frac{\partial \phi_1}{\partial y} \right)_{y=s} - \frac{ds}{dx} \left(\frac{\partial \phi_1}{\partial x} \right)_{y=s} \right\} \tag{A24}$$

The potential both above and below the wax surface $\phi(x,y)$ can then be expressed in terms of the effective charge density as

$$\phi(x,y) = \frac{1}{4\pi\epsilon_o} \int_{-d/2}^{d/2} \phi(r)\, dr \ln \prod_{n=-\infty}^{\infty} \frac{(x - r + nd)^2 + [y + s(r)]^2}{(x - r + nd)^2 + [y - s(r)]^2} \tag{A25}$$

Equation (A25) can be expressed (ref. 22) in terms of hyperbolic and trigonometric cosines

$$\phi(x,y) = \frac{1}{4\pi\epsilon_o} \int_{-d/2}^{d/2} \phi(r)\, dr \ln \frac{\cosh k\,[y + s(r)] - \cos k\,(x-r)}{\cosh k\,[y - s(r)] - \cos k\,(x-r)} \tag{A26}$$

The quantity: $\left(\frac{\partial \phi_1}{\partial y}\right)_s - \frac{ds}{dx}\left(\frac{\partial \phi_1}{\partial y}\right)_s$ can then be obtained by differentiating Eq. (A16). If $\sigma(x)$ is known, the relation which results [taking account of Eq. (A24)] can be regarded as an integral equation for the above quantity, i.e., the induced charge distribution. Solution of the integral equation will then yield the potential distribution throughout space, and the corresponding electrostatic energy integral can then be evaluated. Although in principle, a procedure exists for determining the contour in the absence of surface charge mobility, and which minimizes the surface, strain and electrostatic energy are subject to the condition

$$\int_0^{d/2} (s(x) - s_o)\, dx = 0 \tag{A27}$$

it is not clear that the fruit of such a calculation would warrant the effort necessary to obtain it.

APPENDIX B

Heat Transfer in Holographic Storage Devices

The thermal analysis concerns the structure shown in Fig. 41, where a thin storage layer (typically composed of a thin-thermoplastic layer over a thin-photoconductive layer) is shown deposited on a glass substrate. Typical dimensions are a thickness of 2 to 5 μm for the storage layer, and 3 to 6 mm for the glass substrate. The total lateral extent of the storage plane is at least 10 cm. In operating a holographic-memory system with automatic-page selection, a small area of the storage plane of about 1-mm-diameter is heated; it is the temperature of this small heated region that is of interest.

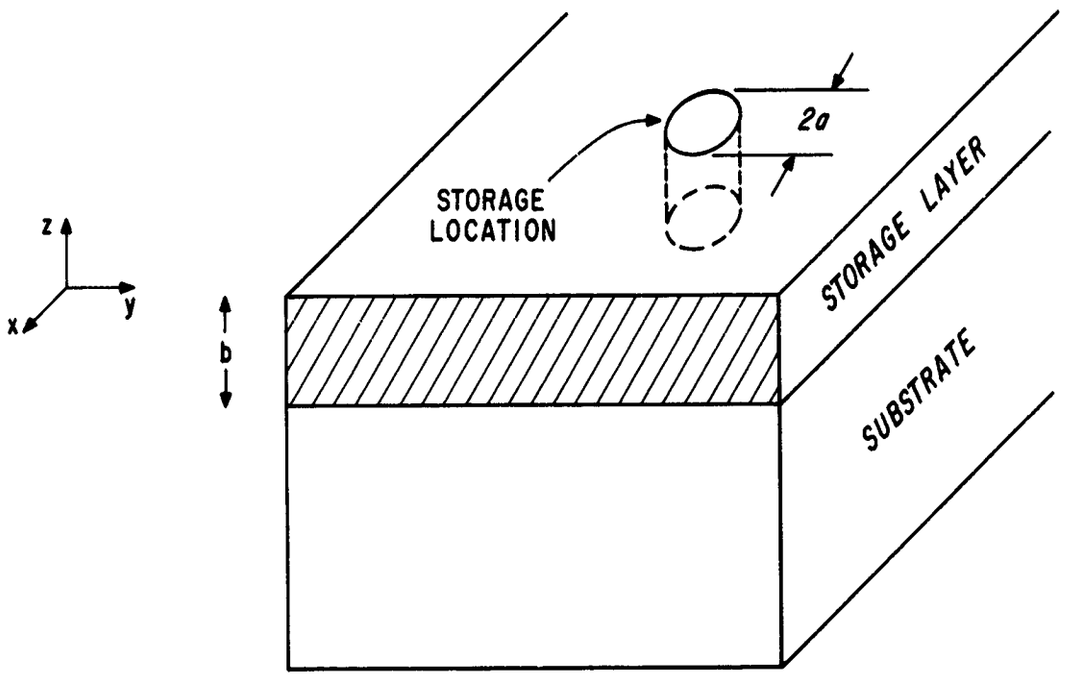

Figure 41. Heat transfer geometry.

Some simplifying assumptions can be made: (1) the storage plane fills the semi-infinite region $z > 0$ (since the area of interest is so much smaller than all other dimensions, this assumption will not significantly change the results); (2) there is no heat flow over the plane $z = 0$ at the top surface of the storage layer (we are thus neglecting heat losses by radiation, but this is a small effect for the small temperature deviations we encounter in thermoplastic recording); (3) the heat is applied uniformly in the volume of the selected region, i.e., the volume bounded by the cylinder $|r| < a$, $0 \leq z \leq b$. (this is exactly the case for a thermoplastic heated by the absorption

of electrons or light, and experimentally appears to be a reasonably good approximation for a resistively-heated spot); and (4) the thermal characteristics of the storage layer (a plastic) and the substrate (a glass) are identical (since the thermal decay times are determined mainly by the substrate, this is a reasonable assumption).

The temperature is found by the aid of the concept of point sources of heat and the method of images. We image a point source of heat somewhere in the volume bounded by $|r| < a$, $0 < z < b$, where 2a is the diameter of the storage area and b is the thickness of the storage layer. We note that if the source point is at the location (x,y,z), the contribution of another equal-strength source located at (x,y,-z) (an image point) will yield a solution to the problem that maintains the boundary condition of no heat flow at the plane $z = 0$. Thus, the solution of the present problem, schematically shown in Fig. 41, may be found by solving the easier problem of the temperature due to heat generated in the cylindrical region $|r| < a$, $-b < z < b$, which is imbedded in an infinite medium. In particular, the temperature at the origin (which is the surface of the storage area in our problem) at the time (t), due to heat generated at the constant rate (A) per-unit-volume per-unit-time is (ref. 21)

$$V = \int_0^t \int_{-b}^{b} \int_0^{2\pi} \int_0^a \frac{A r\, e^{-(r^2 + z^2)/4k(t - t')}}{8\rho c\left[\pi k(t - t')\right]^{3/2}}\, dr d\theta\, dz dt \qquad \text{(B1)}$$

where ρ is the density of the medium, c is its specific heat, k is the thermal diffusivity defined by $k = K/\rho c$ where K is the thermal conductivity. Integrating with respect to r, θ, and z we find

$$V = \frac{A}{\rho c} \int_0^t \left(1 - e^{-a^2/4ku}\right)\left(\text{erf } b/4ku\right) du \qquad \text{(B2)}$$

This integral has been evaluated numerically, and Fig. 42 shows a plot of the temperature versus time for a 10 μsec heat pulse. Note that for this case the temperature 10 μsec after the termination of the heat pulse (i.e., a time equal to the heat pulse) is about one-half the peak temperature, but that the time needed to decay to 3% of the peak value is about 1000 times the heat-pulse duration. These two features, the time to decay to one-half and 3% of the peak temperature can be demonstrated to scale for all heat pulse durations for which this model is valid. The extreme length of time necessary for the temperature to return to ambient may be appreciated by noting that for large times the temperature falls as $1/\sqrt{t}$. These results have been tested experimentally and very close correspondence has been found between this theory and experiments.

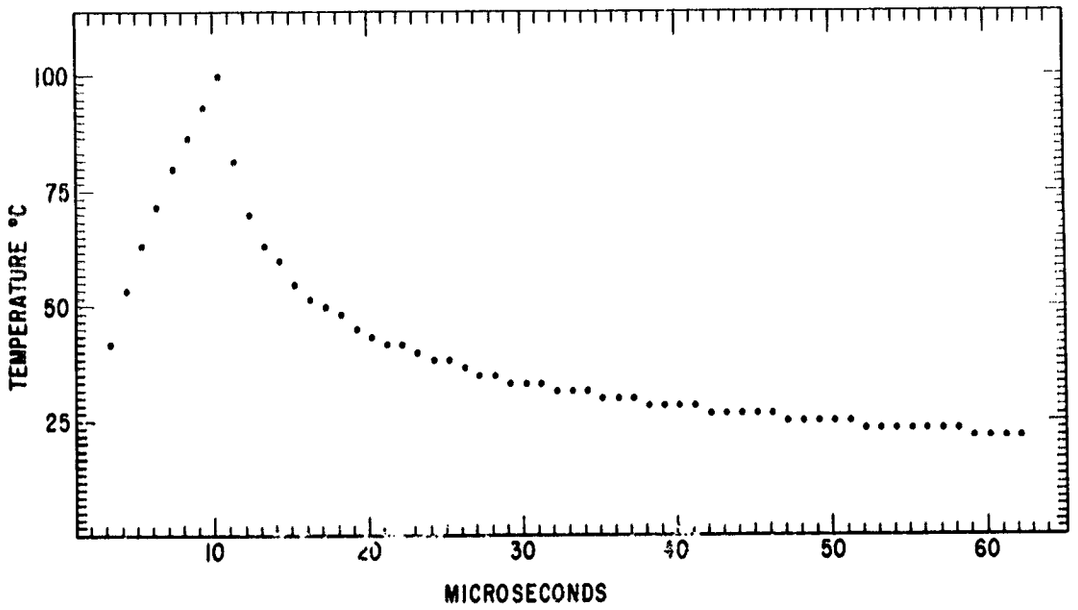

Figure 42. Plot of temperature versus time for a 10 μsec heat pulse.

As stated above, the film may be heated arbitrarily fast. The results above can be used to estimate the energy required to heat the film to a temperature V_o in a time t, but a simpler heuristic argument may also be used.

The energy needed to heat an area of the storage layer to a temperature (V) is

$$Q = \rho c V A h \tag{B3}$$

with Q the total energy, A the cross-sectional area of the storage area, h the depth to which the film is heated, and ρ, c as given above. The energy per unit area, J, is then

$$J = \rho c V h \tag{B4}$$

Note that as we apply heat to the storage area, its effect will not be contained in that area but will spread. For short times we can assume that the heat does not spread laterally along the storage film but rather that most of the heat penetrates into the substrate (this is particularly so if the heat is applied via a thin resistive heater at one surface of the film). The total volume heated during the pulse will then be determined by how far the heat spreads. A good measure of this distance is

$$h = \sqrt{kT} \tag{B5}$$

where k is the thermal diffusivity, defined above, and T is the heat pulse duration. We then find that the energy required is

$$J = \rho c V (kT)^{1/2} \tag{B6}$$

The power required is

$$P = \frac{\rho c V (k)^{1/2}}{(T)^{1/2}} \tag{B7}$$

Thus, the film can be heated to any temperature (V_o) arbitrarily fast, and the energy (E_o) necessary to do this is of the form [Eq. (B6)]

$$E_o^2 = (\text{constant}) \cdot t \tag{B8}$$

However, as shown in Eq. (B2) and Fig. 42, the deformable storage media cools over a comparatively long time period. This theoretical result is confirmed by experimental findings, and shows that the ratio of the cooling to heating time is about 10^3:1. This means that if heat is transferred into a thermoplastic-type storage media in 1 msec, the time required for the temperature to return to its ambient value will be about 1 sec. Thus, the theoretical and experimental results show that the cycle time of a thermoplastic-type holographic-storage medium, where heat must be transferred to and from the storage device, is limited by the time necessary for the temperature of the storage medium to return to its ambient level.

APPENDIX C

HOLOGRAM RECORDING CRITERIA USING PHOTOEMISSIVE MECHANISMS

Assuming the introduction of a differential quantity of charge dq_o along a region of the deformable photoemissive surface (Fig. 43) and allowing some depression along that region in comparison to an adjoining dark region, the capacitance C_1 of the depressed region will in general differ from the capacitance C_2 of the adjoining region because of the differences in separation of the two regions from the transparent electrode. An equivalent circuit is shown in Fig. 44, from which it is apparent that

$$dq_o = dq_1 + dq_2 \tag{C1}$$

$$dq_1 = C_1 dv_1 + V dC_1 \tag{C2}$$

$$dq_2 = C_2 dv_2 + V dC_2 = \frac{v_1 - v_2}{R}\, dt \tag{C3}$$

where V is the dc potential along the surface $>> v_1, v_2$, and where R is the resistance which separates adjoining light-dark regions. Taking the differential force per-unit-area P due to depression as proportional in a first order approximation to the relative displacement where $C_2 < C_1$ occurs both to depression of the light region and dark region elevation due to incompressibility, we have

$$P \equiv 2\zeta\, \frac{x_o - x}{x_o} = \epsilon\left[\left(\frac{V + v_1}{x}\right)^2 - \left(\frac{V + v_2}{2x_o - x}\right)^2\right] \tag{C4}$$

from which

$$\frac{2\epsilon}{x}\left\{\frac{V + v_1}{x}\, dv_1 - \frac{x(V + v_2)}{(2x_o - x)^2}\, dv_2 - \left[\left(\frac{V + v_1}{x}\right)^2 + \frac{x(V + v_2)^2}{(2x_o - x)^3}\right] dx\right\} = -2\zeta\, \frac{dx}{x_o} \tag{C5a}$$

which yields

$$dx \approx \frac{\epsilon E_c}{2\epsilon E_c^2 - \zeta}\, (dv_1 - dv_2) \tag{C5b}$$

where

$$\frac{V + v_1}{x} \quad \frac{(V + v_2)x}{(2x_0 - x)^2} \quad E_c \tag{C5c}$$

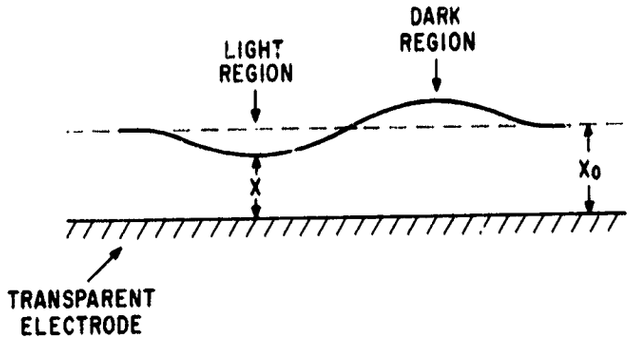

Figure 43. Geometry of deformable photoemissive surface.

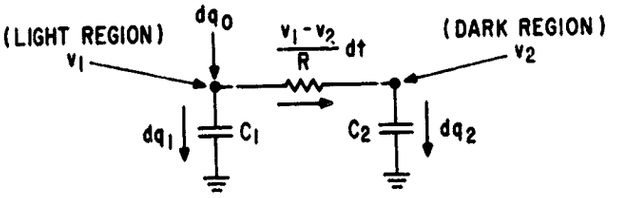

Figure 44. Equivalent circuit of photoemissive holographic region.

Noting that

$$dv_2 = V \frac{dC_1}{C_2} + \tau_2 (v_1 - v_2)\, dt \tag{C6a}$$

with

$$RC_2\tau_2 = 1 \tag{C6b}$$

we have

$$dx \approx \frac{\epsilon E_c}{2\epsilon E_c^2 - \zeta} \left\{ dv_1 - V\frac{dC_1}{C_2} - \tau_2 (v_1 - v_2)\, dt \right\} \tag{C7a}$$

with

$$dC_1 \equiv - dC_2 \tag{C7b}$$

Since

$$dC_1 = \epsilon \frac{A}{x^2}\, dx = - C_1 \frac{dx}{x} \tag{C8}$$

then

$$dx \approx \frac{\epsilon E_c}{2E_c^2\epsilon - \zeta} \left[dv_1 + V\frac{dx}{x} - \tau_2 (v_1 - v_2)\, dt \right] \tag{C9a}$$

and

$$\frac{V}{x}\frac{dx}{dt} = \frac{\epsilon E_c^2}{\epsilon E_c^2 - \zeta} \left\{ \frac{dv_1}{dt} - \tau_2 (v_1 - v_2) \right\} = - \frac{V}{C_1}\frac{dC_1}{dt} \tag{C9b}$$

Noting Eqs. (C1-C3) we then have

$$\alpha v_1' + \beta\tau_1 (v_1 - v_2) = i_o/C_1 \tag{C10a}$$

$$(\beta - 1)\, v_1' + v_2' - \beta\tau_2 (v_1 - v_2) = 0 \tag{C10b}$$

where

$$RC_1\tau_1 \equiv 1 \tag{C10c}$$

and

$$\alpha = \frac{\zeta}{\zeta - \epsilon E_c^2} \tag{C10d}$$

$$\beta = 1 - \frac{\epsilon E_c^2}{\zeta - \epsilon E_c^2} \frac{\tau_2}{\tau_1} = 2 - \alpha \tag{C10e}$$

Equations (C 10a,b) solve for either v_1 or v_2 as

$$\alpha v'' + 2\beta\tau v' = \beta\tau i_o/C \tag{C11a}$$

for which

$$v_1 = A\, e^{-\gamma t} + \frac{i_o t}{2C} + D \tag{C11b}$$

$$v_2 = \beta e^{-\gamma t} + \frac{i_o t}{2C} + E \tag{C11c}$$

with

$$A + D = B + E = 0 \tag{C11d}$$

and

$$\gamma \equiv \frac{2\beta\tau}{\alpha} \equiv 2\tau(1-r) \tag{C11e}$$

where

$$r \equiv 2\frac{\epsilon E_c^2}{\zeta} \tag{C11f}$$

Noting

$$v_1' = \frac{1}{C}\frac{dq_1}{dt} - \frac{V}{C}\frac{dC_1}{dt} \tag{C12a}$$

we find

$$v_1'(0) = i_o/\alpha C \tag{C12b}$$

$$A = -\, i_o R/4 \tag{C12c}$$

$$B = (\alpha/\beta) i_o R/4 \tag{C12d}$$

and

$$v_1 = \frac{i_o R}{4}\left(1 - e^{-2(1-r)t/RC}\right) + i_o t/2C \tag{C13a}$$

$$v_2 = -\frac{i_o R}{4(1-r)}\left(1 - e^{-2(1-r)t/RC}\right) + i_o t/2C \tag{C13b}$$

with

$$\beta/\alpha = 1 - r \tag{C13c}$$

The equations show that for $r > 1$, the potentials $v_1 \neq v_2$ and differential depressions occur, whereas for $r < 1$, the exponential terms rapidly disappear and $v_1 = v_2 = i_o t/2C$ at time periods $t >> RC$. The parameter $r = 2(\epsilon E_c^2/\zeta)$ is a figure of merit for the deformable material, and represents the ratio of electrostatic to elastic stress. Thus materials in which surface depressions occur due to photoemission processes are those where the increase in surface energy necessary for a portion of the film surface to reach the transparent electrode within a half-period of the pattern is less than the electrostatic energy originally stored in the same half-period. It can be shown that

$$x_o - x \approx \frac{i_o R}{8E_c}\frac{r}{r-1}\left[1 + \frac{1}{(1-r)(2-r)}\right] e^{-2\tau(1-r)t} \tag{C14a}$$

from which

$$\epsilon = \frac{RC}{2(r-1)} \ln \frac{8E_c \Delta x}{i_o R f(r)} \tag{C14b}$$

where

$$f(r) = \frac{r}{r-1}\left[1 + \frac{1}{(1-r)(2-r)}\right] \tag{C14c}$$

Equation (C14b) gives the time interval necessary to achieve a depression $\Delta x = x_o - x$. Taking $\zeta \sim 6 \cdot 10^4$ dynes/cm^2 and $E_c \sim 10^7$, then $r \approx 0.1$ indicating that holographic deformation by photoemissive processes will not occur. Noting that the RC time constant is the product of the resistivity per square reduced by twice the number of holographic lines, and the surface capacitance reduced by the same factor, the RC time constant is of the order of 25×10^{-12} second, i.e., a time smaller by at least an order of magnitude than that given by Eq. (C14c) for a 50-nm depression. However, the critical factor requisite for holographic recording via a photoemission mechanism is that $2\epsilon E_c^2$ be greater than ζ, a condition difficult to realize while satisfying constraints of deformation stability.

REFERENCES

1. J. C. Urbach and R. W. Meier, Appl. Opt. **8**, 2269 (1969).
2. J. W. Swan, Proc. Roy. Soc. **62**, 38 (1897).
3. A. M. Thomas, Brit. J. Appl. Phys. **2**, 98 (1951).
4. W. E. Glenn, J. Appl. Phys. **30**, 1870 (1959).
5. W. D. Holden, ASD 61715 (1962).
6. M. Smith and A. Behringer, SPSE Meeting, Cleveland, Ohio (May 1965).
7. R. W. Gundlach and C. J. Claus, Phot. Sci. Eng. **7**, 14 (1963).
8. J. Gaynor and S. Aftergut, Phot. Sci. Eng. **7**, 209 (1963).
9. P. J. Cressman, J. Appl. Phys. **34**, 8 (1963).
10. N. E. Wolff, RCA Review **25**, 200 (1964).
11. H. F. Budd, J. Appl. Phys. **36**, 5 (1965).
12. J. C. Urbach and R. W. Meier, Appl. Opt. **5**, 666 (1966).
13. J. Gaynor and G. J. Sewell, Phot. Sci. Eng. **11**, 3 (1967).
14. R. J. Collier, J. Opt. Soc. Am. **58**, 1548 (1968).
15. L. S. Chang, Phot. Sci. Eng. **12**, 5 (1968).
16. L. H. Lin and H. L. Beauchamp, Appl. Opt. **9**, 9 (1970).
17. H. R. Anderson Jr., et al., IBM J. Res. & Develop., **15**, 140 (1971).
18. T. L. Credelle and F. W. Spong, RCA Review **33**, 1 (1972).
19. K. Kriz, Phot. Sci. Eng. **16**, 1 (1972).
20. J. J. Bikerman, *Surface Chemistry*, (Academic Press, New York, 1958).
21. H. Carslaw and J. Jaeger, *Conduction of Heat in Solids* (Oxford Press, 1959) 2nd. ed. p. 265.